DECLARATION OF AUTHORSHIP

I, Nguyen Thi Dieu Linh, hereby declare that the thesis entitled: "Fabrication and characterization of PMMA/ZrO_2 hybrid nanocomposites towards the application in 3D printing filaments materials" were carried out by myself under the guidance and supervision of Dr. Do Quang Tham and Assoc. Prof. Dr. Nguyen Vu Giang.

I confirm that: All the results are based on data that I have studied by myself and that are true and have not transgressed research ethics. Simultaneously, the data, figures, and results have never been published in any other thesis or diploma.

Ha Noi, September, 2022

Master student

Nguyen Thi Dieu Linh

ACKNOWLEDGMENT

First of all, I would like to express my gratitude to Dr. Do Quang Tham and Assoc. Prof. Dr. Nguyen Vu Giang for their providing guidance, comments and advising me throughout this thesis. Without their motivation and instructions, the study would have been impossible to be done effectively.

The master's dissertation was carried out at the Department of Physico-Chemistry of Non-Metallic Materials, Institute for Tropical Technology, Vietnam Academy of Science and technology.

I would like to thank all scientists in the Department of Physico-Chemistry of Non-Metallic Materials, Institute for Tropical Technology for their help during I carried out my experiments for the thesis.

I am also thankful to the lecturers at the Graduate University of Science and Technology for providing me the knowledge and tools that I need throughout my studies and for writing my dissertation.

And my biggest thanks to my family for all the trust, sympathy, and support for me. I could not forget to say a special thank you to my friends, and all the members of the CHE 2020B class, without their help this dissertation would have not been done.

CONTENTS

ABBREVIATIONS

Abbreviations	Definition
3D	3 Dimensions
3DP	3-Dimensional printing
AIBN	α,α'-azobis(isobutyronitrile)
DLS	Dynamic light scattering
DSC	Differential scanning calorimetry
DTG	Derivative thermogravimetric
FDM	Fussion deposition modeling
FESEM	Field emission scanning electron microscope
FTIR	Fourier transform infrared
$gZrO_2$	PMMA grafted ZrO_2 (PMMA-g- ZrO_2)
$mZrO_2$	ZrO_2 modified with MPTS
MMA	Methyl methacrylate
MPTS	3-methoxypropyl trimethoxy silane
$oZrO_2$	Original ZrO_2 (purchased from Aladdins company)
PMMA	Poly methyl methacrylate
PMMA/ZrO_2	PMMA/ZrO_2 nanocomposites (using $oZrO_2$, $mZrO_2$, $gZrO_2$)
PMMA/$gZrO_2$	PMMA/$gZrO_2$ nanocomposite
PMMA/$mZrO_2$	PMMA/$mZrO_2$ nanocomposite
PMMA/$oZrO_2$	PMMA/$oZrO_2$ nanocomposite
SEM	Scanning electron microscope
TGA	Thermogravimetric analysis
XRD	X-Ray diffraction
PMMA-g-ZrO_2	PMMA grafted ZrO_2

LIST OF FIGURES

LIST OF TABLES

INTRODUCTION

Recently, three-dimensional (3D) printing technology is among the most attractive research fields for scientists. The 3D printing technology allows to create more complex objects and products than tranditional manufacturing processes. The 3D printing technologies are now being developed rapidly, bringing outstanding changes, and applied in the fields of aerospace, automobile manufacturing, mechanical construction, medical equipment, special jewelry, and even complex electronic circuit panels [1][2]. Furthermore, 3D printing technologies can be applied in education fields such as STEM learning, skills development, and increased student and teacher engagement with the subject matter. Polymer and polymer composite materials based on naturally derived polymers (gelatin, alginate, collagen, etc.) or synthetic polymers (polyethylene glycol (PEG), poly lactic-co-glycolic acid (PLGA), polyvinyl alcohol(PVA), etc) have been currently used for printing in the field of biomedical applications [3][4][5][6].

Polymethyl methacrylate (PMMA), or plexiglass is a type of thermoplastic polymer, it belongs to the acrylic family resins. PMMA is widely used in many industrial and life applications. Specically, in the biomedical, PMMA is widely used as an important component of bone cements, and hard contact lenses [7] because of its biocompatibility with human and animal bodies. Zirconia (ZrO_2) is also among the components of acrylic cements with the roles of reducing polymerization shrinkage, modifying mechanical properties and improving wear resistance, radiopacity and biological activity. In the field of 3D printing materials, neat PMMA is less used alone in PMMA 3D printing materials. Several studies have focused on studying polymer blends and composites from acrylic resins and expanding their applicability [8] [9] [10].

Zirconia has been used as a reinforcement filler for many polymers as acrylic polymers, Acrylonitrile Butadiene Styrene (ABS), and epoxy resins. However, it is an inorganic compound in nature, its surface energy differs from that of organic polymer matrix, leading to poorly compatible with organic polymers, and strongly reducing some properties of the polymer/zirconia systems [11]. Therefore, several studies have focused on the enhancement of the interaction between zirconia and polymer by applying a physical or chemical surface modification of zirconia. Most of studies aim to increase the

dispersion of zirconia particles in the organic polymer matrix, or in other words changing the organic affinity of zirconia particles. Many scientific works have been carried out published on the modification of zirconia by organic compounds, the most common of which is trialkoxysilane compound. In addition, a new approach in surface treatment that is radical polymerization method in which modified nanoparticles was copolymerized with monomers, such as methyl methacrylate (MMA) [12] [13].

Currently, there are few publications about using inorganic-organic hybrid materials such as PMMA-g-ZrO_2 to reinforce in PMMA matrix and applied to 3D printing filaments. Therefore, I performed a study entitled: "Fabrication and characterization of PMMA/ZrO_2 hybrid nanocomposites towards the application in 3D printing filament materials".

The aims of this master thesis are: (1) Successful modification of nanozirconia with using 3-mercaptopropyl-trimethoxysilane (labeled as mZrO_2; (2): Successful synthesis of PMMA grafted zirconia nanoparticles (labeled as PMMA-g-ZrO_2, or gZrO_2); (3): Successful fabrication of 3D printing filaments based on PMMA and mZrO_2 or gZrO_2 by using a mini Haake extruder. In additions, characterizations of mZrO_2, gZrO_2 nanoparticles and PMMA/ZrO_2 nanocomposite filaments were performed and the obtained results were also discussed.

CHAPTER 1: OVERVIEW

1.1. Three-dimensional (3D) printing technology and 3D printing materials

Three-dimensional (3D) printing technology is among the most attractive research fields for scientists in recent years. The 3D printing technology can be used to create complex objects and products. In 1984, Charles W. Hull successfully invented a teacup on the first the stereolithography apparatus SLA-1 by himself, and the related patent on stereolithography was issued on August 1984. He was also the co-founder of a 3D Printing Corporation (USA). After that, numerous related inventions by different methods, such that: (1) Selective sintering (SS) was developed by Carl R. Deckard who worked at the University of Texas in 1986. Michael Feygin and colleague at Helisys, Inc. was developed another method "forming integral objects from laminations" by using laminated manufacturing - LM in 1988. (2) Fused deposition modelling (FDM) was developed by Scott S. Crump, at the company Stratasys, Inc. in 1989. (3) Emanuel M. Sachs and coworker, at Massachusetts Institute of Technology, develop "three-dimensional printing techniques", a process of injecting binding agent and coloured ink on a bed of powdered material, using the injectors of a conventional ink-jet printer.

Currently, there are many 3D printing techniques (Table 1), the most popular ones are layered powder melting (PBF) including Selective laser sintering (SLS), selective laser melting (SLM), 3D inkjet printing (3D JP), photochemical embossing (SLG) [14][15][16][17], layered fusion printing (FFF/FDM) in Figure 1.1

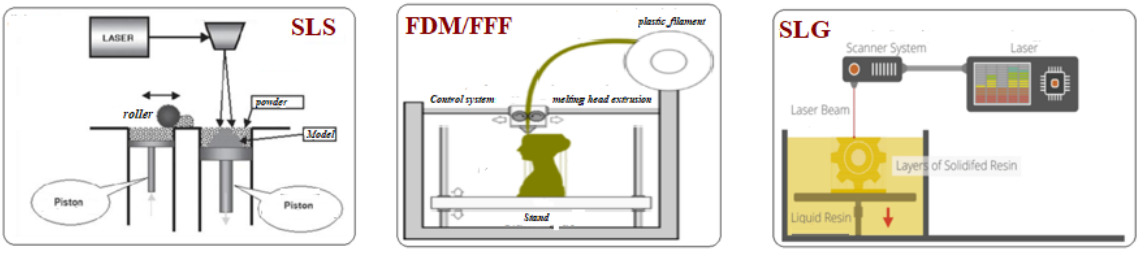

Figure 1.1: Schematic of the 3D printing technique

Three-dimensional (3D) printing technology is widely applied in the world such as automotive industry, construction, models designed, medical equipments, health care, etc. [18]. In the art field, this technology can create special objects and jewelry. In the electronics industry, it is used to make

complex boards. The 3D printing technology is also promoted for many other fields such as education, military, aerospace and so forth.

Table 1.1: Several of 3D printing techniques [5].

3DB	Three-dimensional bioplotter	DCM	Direct composite manufacturing
3DP	Three-dimensional printing	DIPC	Direct inkjet printing of ceramics
AF	Additive fabrication	DLC	Direct laser casting
AM	Additive manufacturing	MD	Material deposition
BM	Biomanufacturing	MEM	Melted extrusion manufacturing
LPD	Laser powder deposition	SL	Stereolithography
LPF	Laser powder fusion	SS	Selective Sintering
LPS	Liquid-phase sintering	SLA	Stereolithography apparatus
LM	Laminated Manufacturing (cutting)	FDC	Fused deposition of ceramics
LMF	Laser metal forming	FFEF	Freeze-form extrusion fabrication
LRF	Laser rapid forming	FLM	Fused layer modeling
LS	Laser sintering	FFF	Fused filament fabrication
JP	Jet prototyping (injection)	FDM	Fused deposition modeling

Figure 1.2 displays the state of the use rate of 3D printing materials with thermoplastics (65%), metal (36%), thermoset resins (29%), sandstone (15%). %), wax (8%) and ceramic/oxide (8%), which excludes food and building materials. The use of metallic materials is also in upward trend as the above report, but polymers (thermoplastics and thermosetting resin) still take into account for the largest proportion [19]. Following the company Statista [20] in Figure 1.2 (b), showing that polylactic acid (PLA) is the most widely used polymer (33%), followed by acrylonitrile butadiene styrene copolyme (ABS) (14%) and thermosetting resin (9%).

For ***FDM/(or FFF)*** printing technique: Thermoplastic filament is melted and extruded, depositing, layer after layer with the desired shape on the bed. The thermoplasticity of polymer filaments is an important property, which allows the filaments to melt during printing and solidify at room temperature after printing. The monolayer's thickness and width, the orientation of the

filaments, and the air gap (between the same layer) are also the machining parameters that affect the mechanical properties of the 3D printing product. If the deformation of products occurs the mechanic properties tend to decrease. The 3D technique for filamentous thermoplastic polymers have some advantages, such as: easy treatment, low cost and using less of material. A number of studies have indicated that significant improvement in mechanical properties can be achieved when using fiber reinforcement for polymers. However, the orientation, bonding between the microfibers and the polymer matrix, and air gap are also the challenges when using polymer composite 3D printing filaments [21][22]. FFM/FDM 3D printing technique is also used to make 3D printed products from polymer blends or polymer composites because of its simplicity and almost similar processing as to pure polymers [23,24]. For 3D printing with polymer materials, due to the monotony of composition as well as features, the number of studies on 3D printing materials from polymers is limited. Most of the research on polymers and 3D printing technology related to the trend surveys, printer testing, and 3D printing techniques. 3D printed products from pure polymers are mainly prototypes, without any special functional product [8][19].

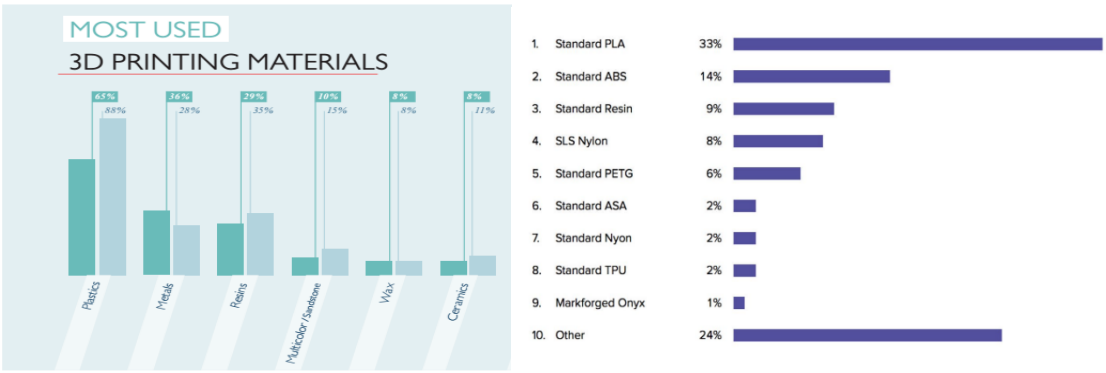

Figure 1.2: (a): Types of 3D printing materials 3D printing; (b): Percentage of common polymers used for 3D printing in the world.

In selective laser melting 3D printing, one by one thin layer of powder is evenly distributed onto a metal plate bed. The laser heat energy is selectively focused on designed areas on the powder bed. After accomplished, the next thin layer is spread down for next process. This printing job is reiterated layer after layer until the model is complete [25]. The residual powder can be recovered

in a variety of ways. The final products may undergo several futher processing stages [26][27][28].

1.2. Introduction to polymer nanocomposite materials

1.2.1. Definition of polymer nanocomposites, hybrid nanocomposites

Polymer nanocomposite is a composite material comprising a polymer matrix and an inorganic dispersent phase that has at least one dimension in nano metric scale inorganic nanoscale building blocks. Nanocomposites combine the advantages of the inorganic material as rigidity, thermal stability, and organic polymer like flexibility, dielectric, ductility, and processability. Moreover, they usually also contain special properties of nanofillers leading to materials with improved properties. A defining feature of polymer nanocomposites is that the small size of the fillers leads to a dramatic increase in interfacial area and some good properties as compared with traditional composites.

A hybrid nanocomposite is a material fashioned by dispersing inorganic nanoparticles into a macroscopic organic matrix. “Hybrid nanocomposites can be distributed into three classes: binary hybrid nanocomposites, ternary hybrid nanocomposites, and multiple hybrid nanocomposites”. A binary hybrid nanocomposite comprises two components containing one nanomaterial; ternary is a composite of three components with one in the nanoscale; and a multiple hybrid comprises more than three components, with at least one of them in the nanoscale. Related to this definition, polymer nanocomposite is one kind of hybrid nanocomposite in which organic matrix is replaced with polymer matrix [29].

1.2.2. Synthesis of polymer nanocomposites

1.2.2.1. Solution method

In this method, all the ingredients and polymer are dissolved in their common solvent by stirring continuously to obtain a homogeneous solution. After that, this solution is poured onto a flat glass plate or Petri dish and complete evaporation of the solvent, the dried membrane is then peeled off from the glass support. Another type of solution method is depositing a thin selective layer, on top of the support, or microporous substrate which may adopt a flat-sheet, hollow fiber, or tubular shape [30].

1.2.2.2. In-situ polymerization

In in-situ polymerization, the nanoparticles must be dispersed in the monomer solution prior to a polymerization process. To ensure the polymer will be formed between the nanoparticles or a good interaction at the interface is obtained. The reason is that the inorganic particles tend to phase separate and sediment quickly from the organic phase [31]. Therefore, organic modification can be performed improve the nanoparticle dispersion. In addition, a variety of techniques such as using heat, using an appropriate initiator can be applied to carry out the polymerization [32].

1.2.2.3. Melt extrusion

This method has number of advantages in relation to the other methods since it is a simple method, no solvent is required, environmentally friendly [33], especially it is a common method used in industrial application [33] [34] [35]. However, the dispersion of nanoparticles is a very important role in this method because of their agglomeration phenomenon. Moreover, high enough temperatures and heat energy are neccessary to be required in the melt extrusion. For a few biopolymers or natural polymers, the degradation temperatures are very close to their processing temperatures [37] [38]. In order over come degradation of the polymer during fabrication, the processing time is should be as shorted as possible, concurrently, enough time is required for the nanoparticles to disperse properly.

1.2.2.4. Other methods

One of the most widely used approach to producing polymer nanocomposite is ultrasonication-assisted solution mixing. Ultrasound is a wave of frequency 2 × 104 to 109 Hz. In this method, the nanoparticles and polymer are initially dissolved in a solution. Thanks to the assistance of the ultrasound, the nanofillers can be well dispersed in the polymer matrix. The polymer nanocomposites are obtained by evaporating the solvent.

1.3. Poly methyl methacrylate (PMMA)

1.3.1. Structure and general properties

Poly methyl methacrylate (PMMA) is known with many different names such as acrylic resin, Plexiglas. It is an important thermoplastic polymer with a transparent plastic material [39], colorless polymer with a vitrification temperature (or reversely, glass transmision temperature) range of 100 – 130°C,

a density at room temperature about 1.2 g/cm^3. This polymer melts at about 130 – 200°C, depending on molecular weight and spatial isomer form. Water absorptivity is 0.3%, moisture absorption is at equilibrium 0.3 to 0.33%, and linear shrinkage mold is 0.003 to 0.0065 cm/cm [40][41][42]. PMMA is among the polymers with high resistance to sunshine. It has very good thermal stability and is known to resist temperatures as high as 100°C and as low as -70°C [40][41]. It also has very excellent optical properties, with a refractive index of 1.49 and is an important component of bone cement because of its biocompatibility with human and animal bodies [7].

PMMA has a high Young's modulus and a low elongation at breakage and high scratch resistance. PMMA has good resistance to many chemicals, unaffected by the aqueous solution of most laboratory chemicals. However, it has a low resistance to chlorinated and aromatic hydrocarbons, esters, or ketone [40][41].

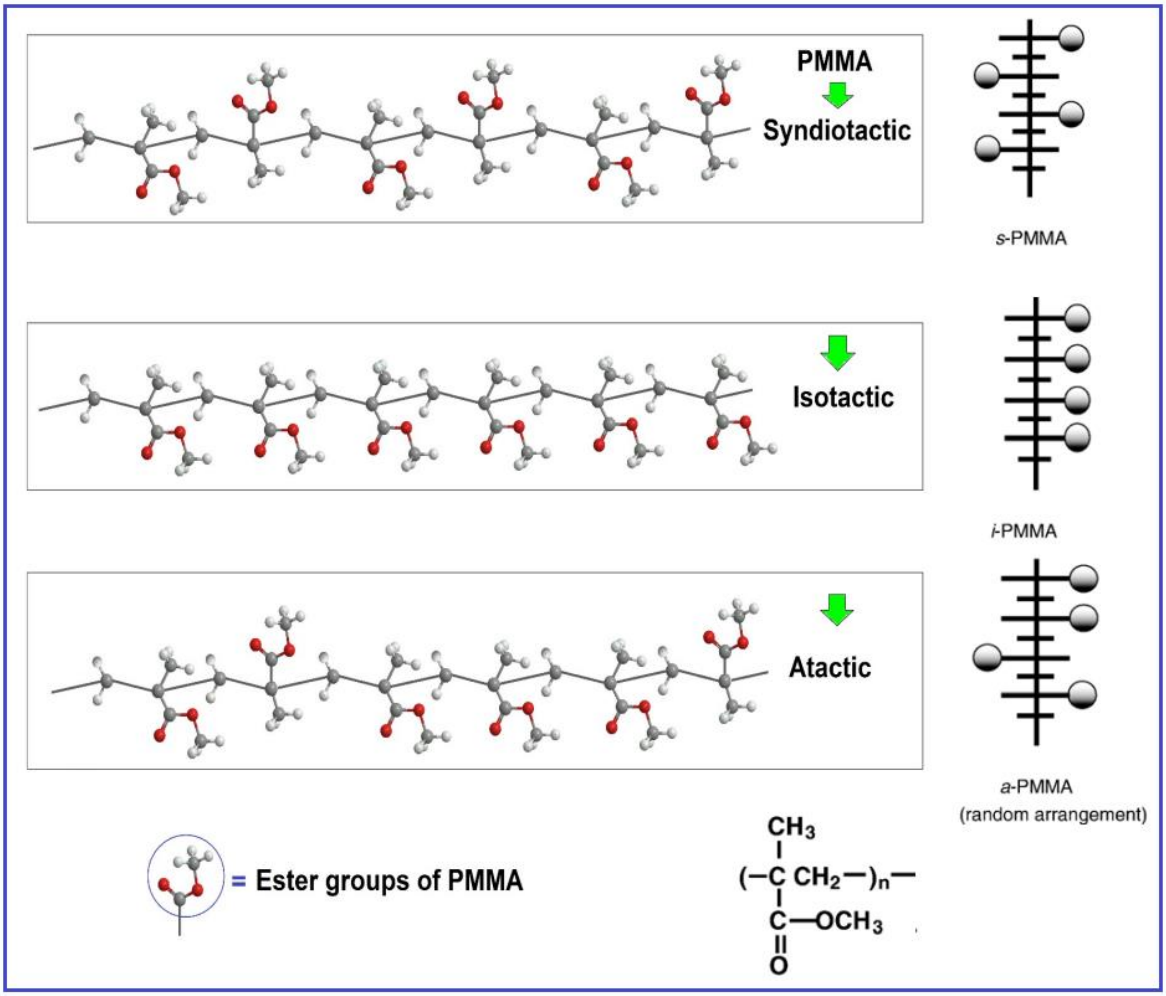

Figure 1.3: PMMA tacticities.

Neat PMMA could be in three types of tacticities: isotactic, syndiotactic, and atactic [43][44]. Pure PMMA might be synthesized in isotactic, atactic, and syndiotactic forms using control/living radical polymerization, reversible addition-fragmentation chain transfer (RAFT), and anionic polymerization, based on the judicious choice of initiator, solvent, and monomer concentration. The amorphous nature of PMMA is controlled by its tacticity in the following order: isotactic < atactic < syndiotactic with the T_g order: 55^{o}C < 120^{o}C < 130^{o}C, respectively [45].

In the chemical field, PMMA is a synthetic polymer from MMA monomer (molecular formula: $C_5H_8O_2$). Methyl methacrylate is a colorless liquid at room temperature, density is 0.94 g/cm^3, boiling point 101^{o}C, melting point -48^{o}C, and viscosity at 20^{o}C is 0.6 cP. Methyl methacrylate reacts with almost esters like hydrolysis and reacts with alkalis since it is an ester. In addition, in the molecule, C = C double bond, methyl methacrylate easily engages in the polymerization process to form polymer (PMMA). The presence of methyl (CH_3) groups prevents the polymer chains from tightly closing in a crystalline fashion and from rotating freely around the C-C bonds. As a result, PMMA is hard plastic, it has a visible light transmission, and since it keeps these properties over years when exposed to ultraviolet radiation and weathering, PMMA is an ideal substitute for glass.

1.3.2. Synthesis of PMMA

Poly (methyl methacrylate) was synthesized by different methods. Five polymerization methods of MMA are mainly used such as bulk, solution, emulsion and suspension polymerizations. There are many PMMA polymerization technologies that mainly appear in basic research, such as controlled radical polymerization (CRP), reversible addition fragmentation chain transfer polymerization (RAFT), nitroxide-mediated radical polymerization (NMP) and atom transfer radical polymerization (ATRP).

1.3.2.1. Bulk polymerization

Bulk polymerization is a simple, rapid and economical method, which only involves a monomer and an initiator as the main components, without any solvent [46]. The reaction of polymerization can be started by using heat or light, then the viscosity of the reaction mixture becomes higher and higher and changing to solid form.

1.3.2.2. Solution polymerization

The solution polymerization method has plenty of advantages such as: environmentally friendly (when the solvent is less toxic) and it is not causing localized heat [31]. But there are also some limitations such as: During the polymerization process, there are some side reactions between the solvent and monomers, which will reduce the average molecular weight of the polymer and it is necessary to revert the solvent and separate the polymer from the solvent at the end of the process.

1.3.2.3. Emulsion polymerization

Emulsion polymerization is generally used in industrial processes. That usually start with the main components concluded monomers, initiators, surfactants, etc. The main role of the emulsifier is to reduce the surface tension between the two monomer aqueous phases, so emulsifiers were added to the system in order to enhance emulsification ability. If water-insoluble monomers are added to the system, part of the monomers will diffuse in the micelles, the rest will be suspended in the solvent. Some common initiators like peroxide, and hydroperoxide compounds, etc.

Polymerization takes place within the micelles. As polymerization proceeds, the micelles grow by adding monomer from the aqueous solution whose concentration is replenished by dissolution of monomer from the monomer droplets. The process continues until other free radicals diffuse into the micelle and cause a termination to form a polymer molecule. The size of polymer molecules gradually increases to some extent. However, polymerization continues to take place in the polymer particles. Such a process forms many polymer droplets.

1.3.2.4. Suspension polymerization

Suspension polymerization is applied in systems in which the monomer and initiator are not soluble in the liquid phase (water or organic solvents). In fact, it also relies on whether we choose water or organic solvent as the continuous phase. Monomer droplets can be created within the liquid matrix and suspended as the viscosity increases under continuous mechanical agitation. The polymerization occurs in the droplets of the dispersed phase, which are used as small-sized reactors, as result, the polymer beads are created. In addition, the process of suspension and polymerization can use surfactants and stabilizers.

Suspension polymerization has advantages over other polymerization techniques because of the following reasons: Water is usually a continuous phase, good heat transfer, temperature and viscosity are easily controlled. Compared with emulsion polymerization, purification and treatment of polymers are much easier because fewer catalysts are used and the final product is 100% resin. The suspension polymerization must be stirred and sufficiently stable to avoid agglomerating the particles and forming large masses. The final product is usually non-stick if the glass transition or melting point is higher than the granule temperature. The final polymeric particles have a particle size in the 0.1-5 mm diameter range and are at least 10 times larger than those produced during emulsion polymerization.

1.3.2.5. Atom transfer radical polymerization – ATRP

"Atomic transfer radical polymerization - ATRP" is a new method used to synthesize a number of polymers, copolymers, and bulk polymers. ATRP was controlled by remaining the balance between the chain-development speed and the deactivation of the ligands.

The deactivating ligands (P_nX) react with the transition metal (Mt^m/L: acting as an activator, at low oxidation state m) with a rate constant of activation (k_{act}) to form the active radical P_n* and the transition metal in high oxidation state (Mt^{m+1}/L) – deactive (scheme Figure 1.5, in which, L is the ligand, Mt^m is the metal M is at a low oxidation state m, Mt^{m+1} is metal at a high oxidation state m + 1). The inactivated element (Mt^{m+1}/L) reacts with the growing radical in the opposite direction with the k_{deact} reaction rate to form (P_nX) and back to the inactive and active state (Mt^m/L). Polymer chains are grown by addition to the same monomers as in conventional free radical duplication, with k_p rate polymerization. Polymer create to PnX is always an action polymer until the catalyst was destroyed, monomer concentration is low or energy supply stops [47][48][49][50].

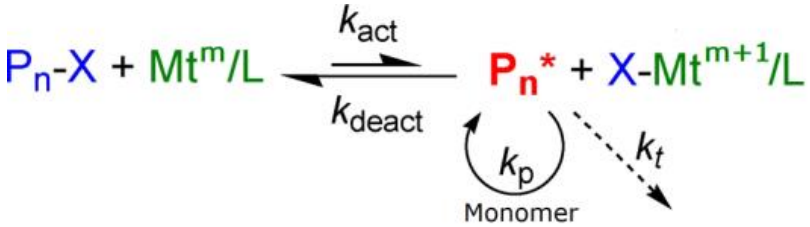

Figure 1.4: Scheme reaction ATRP.

1.3.3. Advantages and disadvantages of PMMA [51]

PMMA is widely used in many different industries thanks to the following its advantages:

Transmittance: PMMA polymer has high light transmittance with refractive index of 1.49. PMMA allows 92% of visible light to pass through it, which is less than common glass but larger than most of other plastics. PMMA can easily be thermoformed without any loss in optical clarity. As compared to polystyrene and polyethylene, PMMA is recommended for most outdoor applications thanks to its environmental stability.

Surface hardness: PMMA is a tough, durable and lightweight thermoplastic. The density of acrylic ranges between 1.17-1.20 g/cm^3 which is half less than that of glass. It has excellent scratch resistance when compared to other transparent polymers such as polycarbonate, but less than glass. It exhibits low moisture and water-absorbing capacity, such products have good dimensional stability.

UV stability: PMMA has high resistance to UV light and weathering. As a result, PMMA is suitable for outdoor applications for long term open-air exposure. Most of commercial acrylic polymers are UV stabilized for good resistance to prolonged exposure to sunlight as their mechanical and optical properties fairly vary under these conditions.

Chemical resistance: Acrylics are unaffected by aqueous solutions of most laboratory chemicals, by detergents, cleaners, dilute inorganic acids, alkalies, and aliphatic hydrocarbons. Nevertheless, acrylics should not use with chlorinated or aromatic hydrocarbons, esters, or ketones.

Sometimes, pure PMMA properties do not meet the property standards from specific applications. Therefore, some co-monomers, additives, or fillers can be used for further enhancement of PMMA properties like impact resistance, chemical resistance, flame retardancy, light diffusion, UV light filtering, or optical effects. For examples:

- Using the co-monomer methyl acrylate enhances the thermal stability by decreasing the thermal degradation during heat processing.

- Plasticizers are added to modify glass transition, impact strength.

- Fillers can be added to modify final material properties or improve cost-effectiveness.

- The dye can be added during polymerization for UV light protection or color decoration.

Besides the excellent properties of PMMA, it also has some limitations such as:

- Poor impact resistance,
- Limited heat resistance (80°C),
- Limited chemical resistance, prone to attack by organic solvents,
- Poor wear and abrasion resistance,
- Cracking under load is possible.

1.3.4. Applications

Thanks to the advantages of PMMA, it was extensively applied in many different fields.

Architecture and construction: Due to its excellent impact and UV resistance, PMMA is widely used in window and door structures, roofs, panels, and so on. It also facilitates good light transmission and water resistance, making it a suitable choice for greenhouse construction. PMMA is also used to build aquatic parks and marine centers.

Automotive and Transportation: PMMA can be used for making windows, automobile windshields, interior, and exterior panels, fenders, etc. In addition, colored acrylic sheet is used in car indicator light cover, interior light cover, etc. It is also used for a ship’s windows (salt resistance) and aeronautical purposes. Besides that, it also brings some new design possibilities for car manufacturers due to its pleasant acoustic properties, outstanding formability and excellent surface hardness.

Electronics: PMMA is widely used in LCD/LED, TV screens, laptops, smartphone displays as well as electronic equipment displays thanks to its excellent optical clarity, high transmission, and scratch resistance. Due to its excellent UV resistance and excellent light transmission allowing high energy conversion efficiencies, PMMA has also used in solar panels as cover materials.

Medical and Healthcare: PMMA is a high purity and easy to clean material so it is used to fabricate incubators, drug testing devices, and storage cabinets in hospitals and research labs. Furthermore, PMMA is also applied as dental cavity fillings and bone cement because of high bio-compatibility.

Furniture: With exceptional properties of PMMA as transparency, toughness, and aesthetics, it is used to produce chairs, tables, kitchen cabinets, bowls, table mats, etc. in any shape, color, or finishing coat.

1.4. Zirconia (ZrO_2)

1.4.1. Structure and general properties

Zirconia, or Zirconium(IV) oxide (ZrO_2) is a white crystalline solid. In nature, it exists as the mineral Baddeleyite with a monoclinic crystalline structure. It is also known as “ceramic steel”, zirconia is chemically inert and it is considered one of the very good restorative materials in medicine, due to its excellent mechanical properties.

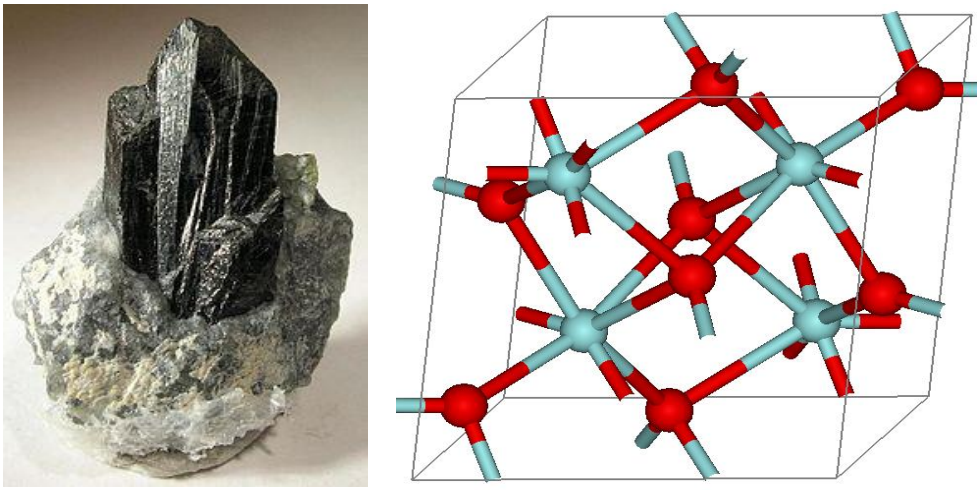

Figure 1.5: Baddeleyite mineral sample and its crystal structure

Among all ceramic materials, zirconia has the highest hardness strength, and toughness at room temperature. At high temperatures, zirconia can be significantly changed in volume during the phase transition, making it difficult to obtain stable products during sintering, thus placing the need for zirconia stabilization.

Partially stabilized zirconia (referred to as PSZ) exhibits excellent physical, mechanical, electrical, chemical, thermal, and bioactive properties. Therefore, it is frequently used as a material for thermal barrier coatings, refractories, oxygen-permeating membranes, and dental and bone implants because of its superior mechanical properties and its similarity to real teeth in mechanical strength [52].

High mechanical resistance:

Zirconium dioxide is known highly resistant to cracking (including further development of cracks) and mechanical stress. Table 1.2 is the other outstanding mechanical property of zirconia:

Table 1.2: Mechanical properties of zirconia [53]

Mechanical properties	Values
Elastic modulus	100 – 250 GPa at 20ºC
Flexural strength	180 – 1000 MPa at 20ºC
Tensile strength	330 MPa at 20ºC
Fracture toughness	10 MPa·√m at 20 °C
Hardness, Vickers	1220
Hardness, Mohs	8 – 8.5

High temperature resistance and expansion:

Zirconium dioxide is widely known for its high resistance to heat with a melting point and thermal expansion coefficient are 2700ºC and 1.08×10-5 K^{-1}, respectively. Thus, the compound has found various uses in refractories and high-temperature industries. Table 1.3 is the different temperature ranges of melting point for zirconia, based on its temperature-dependent forms [53].

Table 1.3: High temperature resistance and expansion [53]

Zirconia's temperature-dependent form	**Melting point**
Monoclinic, baddeleyite	20 – 1170ºC
Tetragonal	1170 – 2370ºC
Cubic	2370 – 2700ºC

However, in the tetragonal form, zirconia may undergo a phase change, where internal stresses arise, and cracks begin to develop. In order to correct this weakness, stabilizers such as yttria are added to help more stable yttria partially stabilized zirconia (*or yttria tetragonal zirconia polycrystalline, YTZP*) [54].

Low thermal conductivity:

"Zirconium dioxide has a thermal conductivity of 2 W/(m.K), which makes it perfect for situations where heat needs to be contained" [53].

High chemical resistivity:

"The substance is chemically inert and unreactive, which works in industries that make use of several chemicals during processing. Nevertheless,

the compound dissolves in concentrated acids such as sulfuric or hydrofluoric acid" [53].

1.4.2. Zirconia fabrication

Depending on the temperature, the production of zirconium dioxide may result in three possible phases: monoclinic, tetragonal, and cubic. This unique property of zirconium dioxide provides the flexibility of use in a wide variety of purposes and industries.

Zirconia is produced through thermal treatment, or thermal dissociation, although doing it in its pure form may cause abrupt phase changes that may crack or fracture the material. That is when doping with stabilizers, such as magnesium oxide, yttrium oxide, and calcium oxide is applied to keep the structure intact. This thermal process is also referred to as dry calcination.

Zirconia can also be produced by decomposing zircon via fusion with compounds such as calcium carbonate, calcium oxide, sodium carbonate, magnesium oxide, and sodium hydroxide.

Chlorination of zircon also leads to the production of zirconia, where the resulting zirconium tetrachloride is calcined at a high temperature (~900ºC), producing a commercial grade of zirconia. Another way is to dissolve the collected zirconium tetrachloride in water to form crystallized zirconyl chloride. This resultant is then thermally treated at a high temperature to produce high-purity zirconia [55].

1.4.3. Application

- Ceramics: Thank to the mechanical strength, resistance of zirconium dioxide and high hardness factor of zirconia, so it becomes a suitable component for ceramic manufacturing.

- Refractory materials: Due to its high thermal resistance, zirconium dioxide is used as a component in crucibles, furnaces, and other high-heat environments. In addition, zirconium dioxide boosts the fireproof properties of ceramics like refractory bricks and armour plates. Moreover, zirconia can be used to produce siloxide glass by adding to melted quartz, which is a harder and more stress-resistant glass than quartz opaque glass [56]. Zirconia can also combine aluminum oxide to be used in components for steel casting process.

- Thermal barrier coating: With the compound's low thermal conductivity and high heat resistance of zirconium dioxide it is applied as a coating for jet

engine components which are exposed to high temperatures. The number of studies have confirmed the effectiveness of zirconium dioxide for thermal barrier coating applications, as long as the material is applied properly and uniformly.

- Dental industry: Zirconia is among popular components used in dental, mainly in dental restorations for bridges, crowns, and feldspar porcelain veneers and dental prostheses due to its biocompatibility, good aesthetics, and high mechanical properties. In addition, Yttria-stabilized zirconium dioxide is also instrumental in producing near-permanent zirconia crowns.

- Abrasive material and scratch resistant: Zirconia is being used as an abrasive material because of its elevated mechanical stability and abrasion resistance.

- Jewelry industry: Cubic zirconia has evolved as a viable alternative to diamond (which is extremely expensive). Apart from its durability and strong aesthetic similarity to diamonds, cubic zirconia produces cutting line unlike diamonds and has optical flawlessness that appears completely colorless to the naked eye. It is commonly referred to as a diamond imitation rather than a synthetic diamond, as it resembles a natural diamond visually but does not have the same chemical properties. For examples, cubic zirconia rings and cubic zirconia earrings [56].

1.5. The research status on 3D filaments from PMMA and its composites

Although 3D printing materials based on polymers and thermoset resins have received much research attention, PMMA and the curing acrylic resin family have received little research attention. The reviewed literature shows that the number of studies on 3D printing materials based on polymers such as PLA, ABS, PA is larger than that of PMMA and the number of studies on epoxy resin is larger than that of acrylic resin [22] [24] [57] [58]. PMMA is a hard plastic with a high melting point and shrinkage, which is a limitation when it is used as a printing material. Therefore, number of studies had focused on polymer blends and composites from acrylic resins, with the aim of extending their applicability [8] [9] [10].

Polzin C. et al. [59] studied 3D printing materials based on polymer blend PMMA/polyethylmethacrylate (PEMA). The powder material was a mixture of 50 μm average particle size and a little amount of benzoyl peroxide (BPO)

initiator. The binding liquid was a mixture of hexane-1-ol, 2-ethylhexyl acetate, and hexyl acetate. The authors used a VX500-type 3D printer (Voxeljet Technology GmbH, Augsburg, Germany). The printer's resolution in the x, y, and z axes was set at 64 × 102 × 150 µm, meaning that the thickness of a powder layer was 150 µm, the ink droplet was adjusted to a weight of 90 µg. The powder cavity was lowered and a new layer was spreaded after each xy plane was finished printing. The testing results of the properties of 3D printed products showed that the tensile strength (TS) reached 2.91 MPa, the elastic modulus (YM) reached 233 MPa. When the samples were heat-cured with epoxy resin, the mechanical properties of the product were further improved, the TS reached 26 MPa and YM reached 1990 MPa.

Roca A. et al. [27] indicated that it was difficult to use PMMA as a tissue culture material without treating the its surface. The authors fabricated poly(MMA-co-BMA)-polyethyleneglycol diacrylate (PEG-DA) frame materials from MMA, BMA, PEGDA as curative agents, and photoinitiator ethyl-2,4,6 -trimethylbenzoyl-phenylphosphinate (TPO) as a photoinitiator and using a UV lamp at 365 nm wavelength for 60 min. The results showed that BMA and PEGDA content changed the mechanical properties of the obtained films. The cytotoxicity test showed that the membrane met the cell culture requirement. Therefore, the author proposed to use SLS 3D printing technique to fabricate cell/tissue culture membranes from this material.

Wagner A. et al. [10] studied and fabricated a 3D inkjet formulation to create 3D porous objects for the application requirements of lightweight materials. This ink had an acrylic composition modified with a blowing agent (BA). The purpose of the study was to create porous objects directly during the printing process without the need for foaming treatment steps like current foaming 3D printing techniques. The important characteristics of the ink under the investigation were the viscosity, the decomposition of the foaming agent, and the ultraviolet (UV) polymerization of the base ink. Acrylic foaming ink was made by dissolving BA agents in liquid acrylic resin (PEG-600-diacrylate, PEG600DA) and other additives. After UV irradiation combined with heat, photopolymerization and gas generation occurred simultaneously, resulting in acrylic polymer foam material was formed. This ink is suitable for the Polyjet™ 35 printing technique.

In Vietnam, 3D printing technology has also been deployed in some scientific field, such as, medicine, fine arts, fashion, architecture, mechanics, and education. There have been a number of companies and business services investing to the field of 3D printing technology. Some authors have published their studies related to the overview of research on 3D printing technology. Authors Nguyen Xuan Chanh, Tran Minh Tam, and Nguyen Manh Quan represented introductory reports on 3D printing technology, which briefly described 3D printing techniques and the areas of application, but the reports did not refer to the application of 3D printing technology in Vietnam [18]. Science and Technology Information and Statistics Center in Ho Chi Minh City with the work of Dr. Hoang Xuan Tung, Huynh Huu Nghi, and Vo Hong Ky had a summary report analyzing the trend of 3D printing technology and application in the future. In the report, the authors emphasized the applications of 3D printing technology at the Faculty of 3D Printing Technology of Vietnam National University, Ho Chi Minh City. Modern 3D printers have been applied to test an investigation and many high-quality 3D printing products have been introduced.

From the source data of Sculpteo and other sources, it was shown that three 3D printing techniques, SLS (33%), DFM (36%), and SLS (25%) are the most used within 1000 companies involved in 3D printing were consulted. The number of inventions related to 3D printing also increased dramatically between 2012 and 2017, the number of inventions in 2017 (7141) was double with that of 2016 and three times with that of 2015. 3D printing technology is a research direction that is very interesting in the current period.

At the Institute for Tropical Technology (ITT) in the period 2019-2020, Hoang Tran Dung had performed a research project on manufacturing 3D printers and some 3D printing inks oriented the application in electrical-electronic industry. The results of the project exhibited a 3D printer system and a 3D printing ink. Regarding these topics, the authors had several publications in the journal VAST [28,60–62]. In these reports, a 3D printer that used PLA filament was fabricated [62], an ink containing carbon nanotubes (CNTs) carrying ferromagnetic oxide was synthesized [61] and the ink was used to make electrical supercapacitors by the 3D printing system [60].

P.X. Lan. et al. [63] Hanoi University of Science and Technology fabricated the frame material from poly(propylene fumarate)/diethylene fumarate (PPF/DEF) with the orientation of application in bone tissue engineering. This material was modified by immersion in simulated body fluid (SBF) solution to coat a layer of apatite. The post-denaturation material was implanted with MC3T3-E1 osteogenic cells. Study results showed that the fabrication of PPF/DEF skeleton by stereolithography and SBF modification was suitable for bone tissue culture.

D.X Phuong at Nha Trang University and Park H.-S (Korea Ulsan University) had made smart metal molds for plastic processing using 3D printing techniques SLS [64]. Ha Thuy Tran Thi, Nguyen Dac Hai, and colleagues at Hanoi University of Industry studied, designed, and manufactured a 2-axis tilt-angle condenser sensor using a 3D printer of Stratasys company (USA). With this technology, the sensor had high quality, uniformity, low cost, and met some requirements of conventional sensors. Author Tran Ngoc Hien (University of Transport) had found the optimal operating mode for a type of 3D printing device using commercial PLA and ABS plastic filaments [65].

Based on an overview of the research status on 3D printing technology and 3D printing materials in Vietnam, it can be seen that Vietnamese scientists and technologists have been interested in this field. Most of studies only concentrated at an overview level, introduced the research status on 3D printing in the world, some of studies made some investigations with the commercial polymer filaments, manufacture of 3D printers, preparation of 3D printing ink for capacitors. The amounts of studies performed by Vietnamese authors related to the fabrication of new 3D printing materials from polymers is limited. Nevertheless, there are several inventions related to 3D printing technology registered in the Intellectual property office of Vietnam [66].

In the biomedical, PMMA is a well-known polymer with promising properties that are widely used as an important component of bone cement, and acrylic cement [7, 50] because of its biocompatibility with human and animal bodies. However, it has some limits due to its low thermal stability and brittle property. In order to improve those properties, PMMA can be combined with with inorganic nanoparticles to obtain polymer nanocomposites [5]. Numerous kinds of research indicated that inorganic nanoparticles influence the

mechanical properties of PMMA based nanocomposites. However, using the inorganic components with high content, the organic particles tend to agglomerate in the polymer matrix, thus decreasing the material's properties. Therefore, a variety of researchers have reported on the modification of zirconia by organic compounds, the most common of which is trialkoxysilane moiety for improving its compatibility with the polymer matrix and its dispersity at the nanoscale in the polymer matrix. As the result, they can form covalent bonds with acrylic monomers during polymer synthesis to create hybrid materials. Jiaxue Yang. et al. [67] investigated the effects of 3-aminopropyltriethoxysilane (APTES)- or (3-mercaptopropyl)trimethoxysilane (MPTS) conditioned nanozirconia fillers on the mechanical properties of Bis-GMA-based resin composites. The composites containing the modified nano zirconia improved the mechanical properties of Bis-GMA-based resin composites. Dan Li et al [68] also used vinyltrimethoxysilane (VTMS) to modified asymmetric alumina support zirconia and then grafted vinyl acetate (VAc). FTIR and TGA analytical techniques proved that the VTMS and PVAc chains were successfully grafted onto the ZrO_2 surface.

In the literature, there are some publications related to inorganic-organic hybrid materials like PMMA grafted ZrO_2 nanoparticles, which showed that PMMA grafted ZrO_2 can enhance some properties of PMMA. However, the number of manufacturing publications on hybrid materials from modified zirconia to enhance the interaction with polymer matrix is limited. I have carried out the research entitled: ***"Fabrication and characterization of PMMA/ZrO_2 hybrid nanocomposites towards the application in 3D printing filament materials".***

CHAPTER 2: EXPERIMENTAL

2.1. Materials

Zirconia nano particles (ZrO_2, 99.9%) in white color with density (d = 5.68 g/cm^3), particle size of 20 - 80 nm was provided by Aladdins Chemical Corporation (Shanghai, China). Methyl methacrylate (MMA, 99%, contains ~ 30 ppm MeHQ), α,α'-azobis(isobutyronitrile) (AIBN, 98 %), 3-(trimethoxysilyl) propyl methacrylate (MPTS, 98%) were purchased from Sigma-Aldrich (USA). MMA was removed the MeHQ inhibitor by passing it through a column filled with basic alumina. Acetone (99.7%), ammonia (28%), methanol (99.7%), ethanol (99.7%), 1,4-Dioxane (99.5%) were the reagent grade products of Guangzhou Chemical Company, Ltd., (Guangzhou, China).

PMMA (poly methyl methacrylate) or ACRYPET-VH001 was a product of Mitsubishi (Tokyo, Japan) with melt flow index of 5.7 (load 3.8 kg, at 230^{o}C) and density of 1.19 g/cm^3.

2.2. Sample preparation

2.2.1. Surface modification of ZrO_2 nanoparticles with MPTS

Into a 500 mL round bottom flask, 100 g of nano zirconia was mixed with 200 mL methanol and 20 mL dioxane, the mixture was continuously stirred for 30 minutes. An amount of 2 mL ammonia solution (28%) was added to adjust the pH of the solution to a value of 8.5 ± 0.2. In a 20 mL vial, 10 g MPTS was dissolved in methanol and water at Methanol:H_2O:MPTS weight ratio of 6:2:1. Next, the MPTS solution was slowly injected into the bottom flask through a syringe-needle for about 2 minutes. The mixture in the flask was stirred continuously for 24 hours at room temperature (from 23 - 27 °C) to allow the grafting reaction between MPTS and ZrO_2 nanoparticles proceeded. Residual MPTS after surface treatment was removed from the mixture by 3 cycles of washing with methanol/dioxane and centrifuging with a speed of 6000 rpm and cleaning, following by drying in a vacuum oven at 40 °C to a constant weight. Finally, the solid part was ground by an agate pestle mortar set to obtain modified ZrO_2 nanoparticles (labeled as mZrO_2).

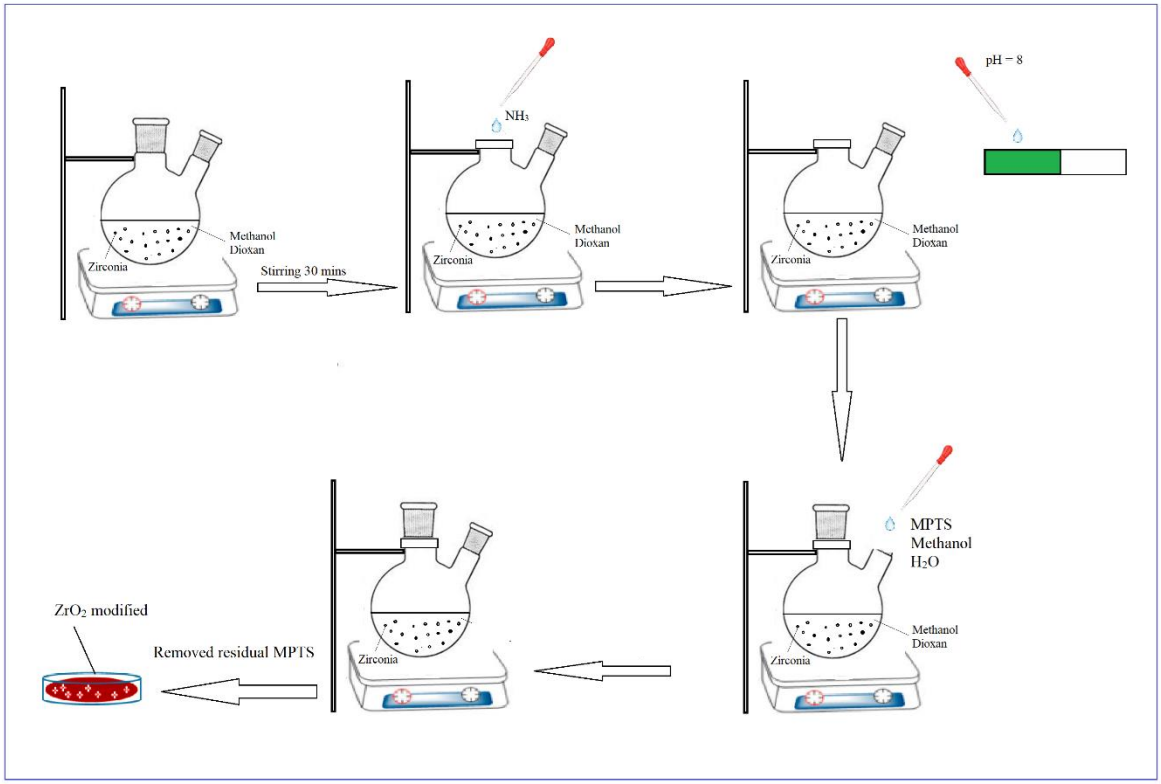

Figure 2.1: Modification procedure ZrO_2 by MPTS.

2.2.2. Synthesis of PMMA-grafted ZrO_2 nanoparticles

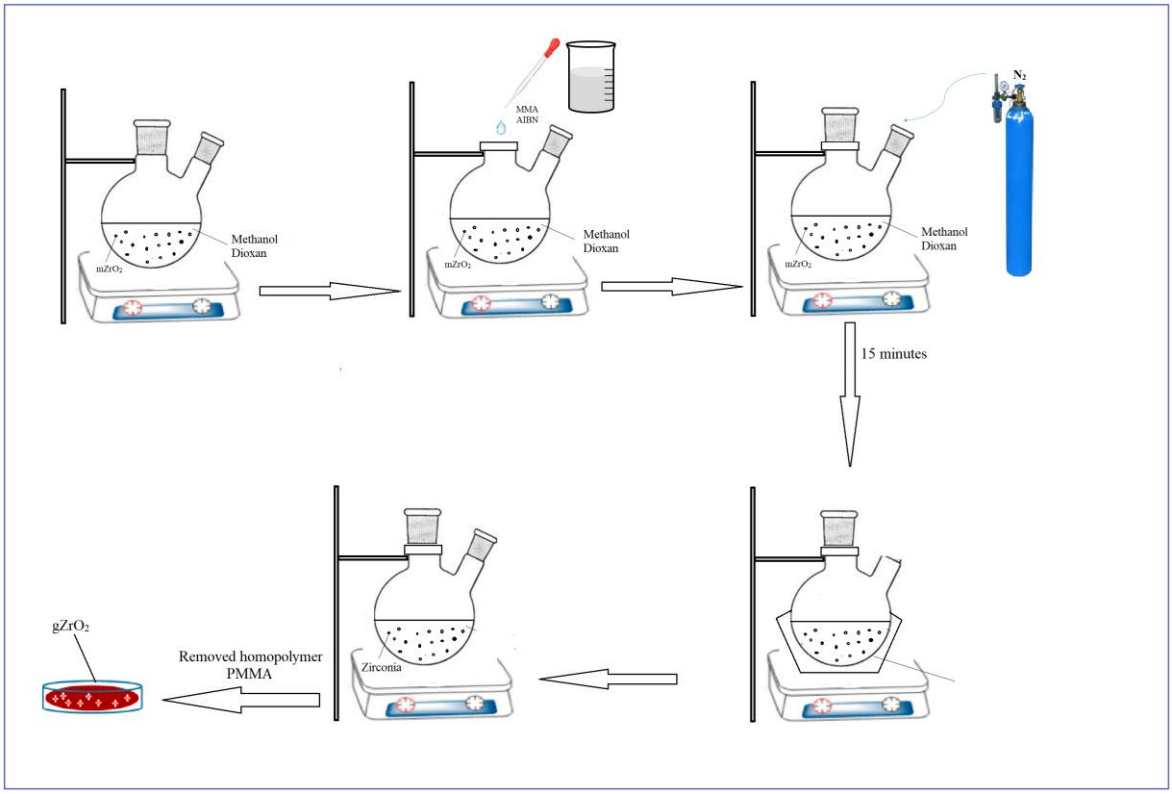

Figure 2.2: Synthesis of PMMA-grafted ZrO_2 nanoparticles.

Into a 500mL round-bottom flask: were added 50 gram $mZrO_2$, 100 mL dioxane, 100 mL methanol, 5 g MMA and 0.05 g AIBN and magnetic stirred

at 15 minutes in the atmosphere of nitrogen. Next, the flask was placed in silicon oil at 60 °C. In this process, the reaction of polymer grafting occurred. After 8 hours the flask was cooled with water. The PMMA homopolymer can be easily separated from the PMMA-g-ZrO_2 when using the solvent mixture. The reason was the PMMA homopolymer soluble in dioxane, and methanol solvents with appropriate concentrations to reduce the viscosity of the solution, which is beneficial for the extraction process. The grafted particles were centrifuged at a speed of 6000 rpm and rinsed with acetone to remove most of the PMMA homopolymer. The solid part was ground by using an agate pestle-mortar set to obtain the PMMA-g-ZrO_2 grafted nanoparticles ($gZrO_2$), followed by drying at 100 °C for 24 h in a circulating hot air oven.

2.2.3. Preparation PMMA/ZrO_2 hybrid nanocomposite 3D printing filaments

Neat PMMA and ZrO_2 were dried at 100 °C for 2 hours in a hot air oven. The mixture of dried PMMA and ZrO_2 with predetermined contents were physically mixed together before adding into the hoper of the a single-screw extruder (Haake Rheomix 252p). The extruder has 4 heating zones, the L/D ratio of 25:1 (L = 475 mm, D = 19 mm). In a general procedure, the extruder was heated at a temperature profile of 190-200-210-210°C, respectively. The PMMA/ZrO_2 nanocomposites were extruded at a rotor speed of 80 rpm through a 2.5-mm circular die, extruded filaments were cooled with air and drawn at a constant speed for diameter of 1.75 ± 0.05 mm.

Figure 2.3: Haake Rheomix 252p machine.

2.2.4. Preparation testing samples by Haake MiniJet machine

Samples in beam or dumbbell shape were prepared by using a Haake MiniJet piston injection molding machine (Figure 2.3 a), with controlling the temperature of the piston chamber at 220 °C, mold temperature of 100 °C and a pressure of 650 bar. Samples in beam shape have dimensions (width, height, length) of 63.4 × 12.8 × 3.2 mm. Samples in dumbbell shape were prepare with the type IV mold in ASTM D638, the narrow section width of 6 mm.

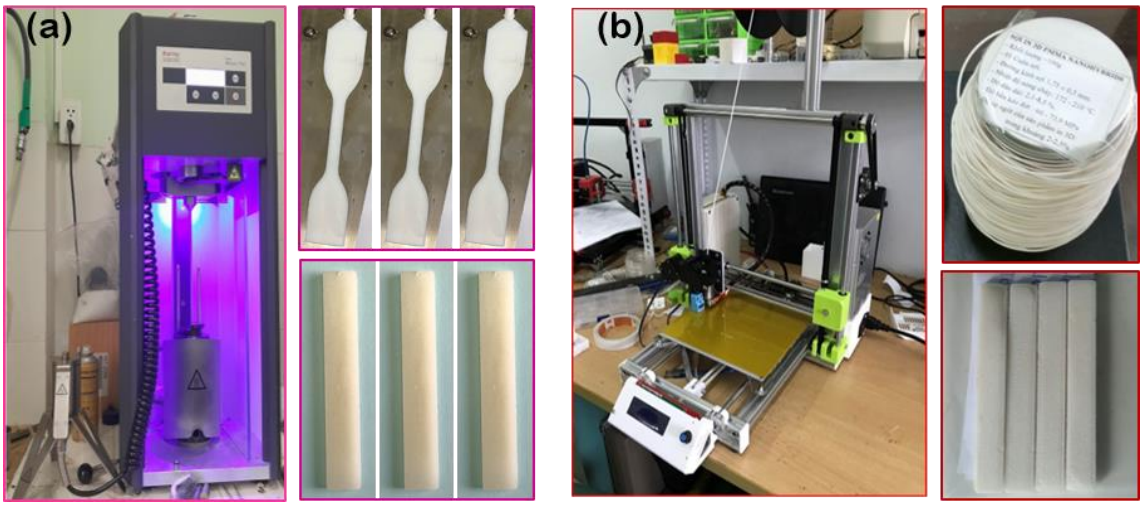

Figure 2.4: (a): Haake MiniJet, (b): FDM 3D printer and testing samples

2.2.5. Preparation testing samples via fusion deposition modeling 3D printer

Samples with dimensions of 12.8 × 70 × 3.2 mm were prepared by using the FDM 3D printer that was the product of the project at the Institute for Tropical Technology [68]. The extruded filaments in section 2.2.3 were loaded into the piston chamber, then pulled through the nozzle of 3D printer preheated at 220 °C. The polymer was melted and extruded and when the nozzle was moving with a design, the melted polymer was deposited on the bed of the printer (preheated at temperature of 100 °C and using an adhesive agent for the first molten layers can adhere to the bed). The appropriate nozzle moving speed was set at 40 mm/min. Each kind of 3D printing filament was printed at least 6 samples, the samples was then stored at room conditions for at least 7 days before testing mechanical properties.

2.3. Characterization measurements

2.3.1. Fourier-transform infrared spectroscopy

FTIR spectra of all samples were performed on a Fourier transform infrared spectrometer (Nicolet iS10. Thermo Scientific - USA) as Figure 2.5 at the Institute for Tropical Technology Vietnam Academy of Science and Technology with 32 scans 4 cm^{-1} resolution. and in wave number ranging from 4000 to 400 cm^{-1} at room temperature.

Figure 2.5: Fourier transform infrared spectroscopy (FT-IR), Nicolet iS10, Thermo Scientific – USA.

2.3.2. Tensile properties

The tensile properties of the composite samples were conducted on a universal mechanical testing machine (Zwick V.2.5. Germany) with a crosshead speed of 100 mm/min. in accordance with ASTM D638 for plastic materials.

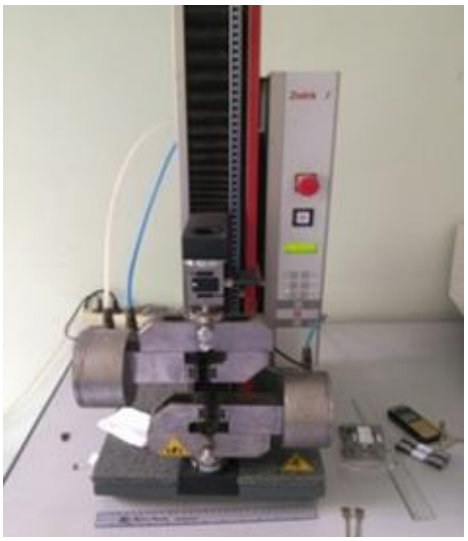

Figure 2.6: Zwick Z2.5 universal mechanical testing machine (Germany).

2.3.3. Flexural properties

Four-point flexural test was performed with a crosshead speed of 5 mm/min, in accordance with ISO 5833:2002 standard with at least 3 testing samples for a test. Molding shrinkage was conducted via measuring the length dimension of cooled testing samples compared with that of the mold.

2.3.4. X-Ray diffraction spectra

The crystalline structures of zirconia powders were examined by X-ray diffraction (XRD) on a Bruker-D5005 instrument (Germany) at the Materials Military Institute of Science and Technology (Vietnam).

2.3.5. Field Emission Scanning Electron Microscopy

The morphology of investigated zirconia particles and PMMA based nanocomposites was observed by using a Hitachi Field Emission Scanning Electron Microscopy (FESEM S-4800) at electron accelerating voltage of 5 kV.

2.3.6. Dynamic light scattering (DLS)

The particle size distribution of zirconia particles in isopropanol (at 1 wt.% solid content) was conducted via dynamic light scattering (DLS) method using a Zetasizer Ver 620 Instrument (Malvern Instruments Ltd.) with laser light source wavelength of 532 nm at 25 ± 0.2 °C.

Figure 2.7: Dynamic light scattering (DLS) instrument.

2.3.7. Thermal Gravimetric Analysis (TGA)

Thermal Gravimetric Analysis (TGA) measurements of the PMMA, zirconia nanoparticles and PMMA/ZrO_2 nanocomposite filaments were carried out by using a NETZSCH TG 209F1 Libra instrument (Netzsch Munich Germany) under nitrogen gas with a flow rate of 40 mL/min from 30 °C to 700 °C a heating rate of 10 °C /min and a specimen weight of about 6 - 7 mg.

CHAPTER 3: RESULTS AND DISCUSSIONS

3.1. Characterization of ZrO_2 nanoparticles modified with MPTS

3.1.1. Fourier-transform infrared spectroscopy

The FTIR spectra of the two kinds of original and modified zirconia nanoparticles ($oZrO_2$, $mZrO_2$) and pristine MPTS liquid are represented in Figure 3.1. Figure 3.1a shows the stretching (ν) and bending (δ) vibrations of OH groups of zirconia at 3443 and 1626 cm^{-1}, respectively. The peaks at 747 and 574 cm^{-1} are assigned for stretching vibrations of the Zr-O group, its bending vibration occurs at the wavenumber of 504 cm^{-1} [69]. The FTIR spectrum of $mZrO_2$ (Figure 3.1 b) shows the presence of the characteristic bands for MPTS such as ν(C=O) at 1726 cm^{-1}; ν(C=C) at 1633 cm^{-1}; δ(CH_3) and δ(CH_2) at 1442 cm^{-1} and 1387 cm^{-1}, respectively. It is worthy to note that residual MPTS had almost removed by washing and filtering processes. Therefore, it is reasonable to suggest that MPTS has been grafted onto surface of ZrO_2 nanoparticles as illustrated in Figure 3.2a.

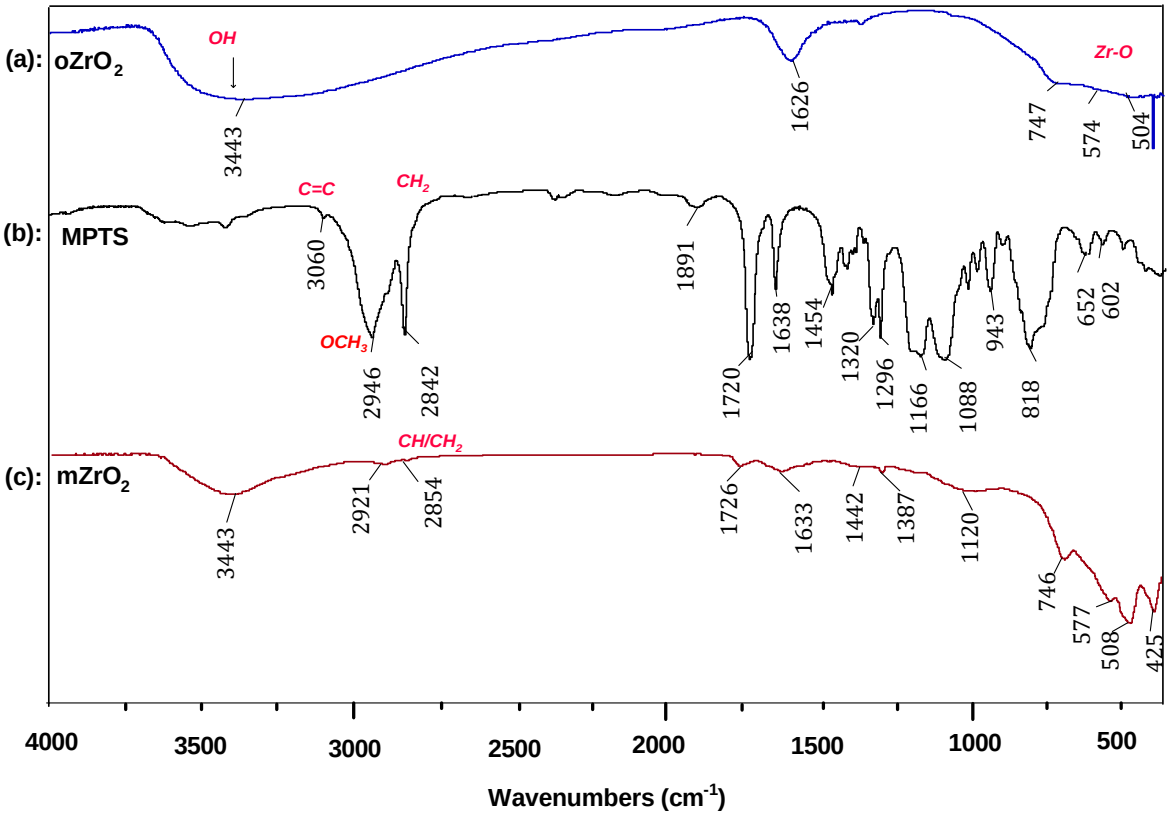

Figure 3.1. FTIR spectra (a) $oZrO_2$, (b) $mZrO_2$ and (c) MPTS.

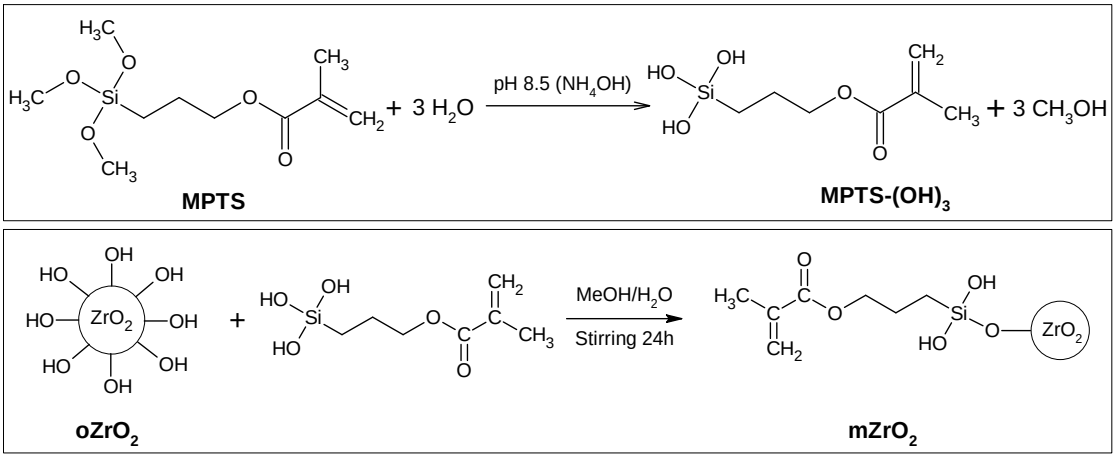

Figure 3.2. Reaction scheme of (a): MPTS hydrolysis and (b): MPTS grafting onto ZrO_2 nanoparticle.

3.1.2. Thermal Gravimetric Analysis (TGA)

Figure 3.3 displays the TGA and DTG curves of $oZrO_2$ and $mZrO_2$ samples in the temperature range from 30 to 700 °C, showing the two main stages of thermal decomposition. The first stage (I) occurs minorly from 30 °C to 180 °C with low weight loss that is attributed to the physical adsorption of water. The second stage (180 °C – 700 °C) is mainly the decomposition of organic molecules that are covalently bonded ZrO_2 nanoparticles. The grafted contents of MPTS on the surface ZrO_2 nanoparticles can be evaluated from TGA measurement data as followed. MPTS has a molecular weight M_{MPTS} = 248.35 g/mol the loading amount of MPTS is 10 grams MPTS for 100 grams of $oZrO_2$ (10 wt.% or 0.403 mmol/g). The molecular weight of MPTS after hydrolysis M'_{MPTS} is 206.27. Thus, the weight percentage of MPTS grafting can be calculated as 2.50 wt.% (Eq.3) [69].

$$\Delta m = \Delta W_M - \Delta W_w = 2.945\% - 0.3822\% = 2.554\ \% \quad (1)$$

$$\text{MPTS grafting content in mol} = \frac{\Delta m(\%)}{206.27} \times 1000 = \frac{25.54}{206.27} = 0.124\ (\frac{\text{mmol}}{\text{g}}) \quad (2)$$

$$\text{MPTS grafting perentage} = \frac{0.124 \times M'_{MPTS}/1000}{0.124 \times M'_{MPTS}/1000 + 1} = \frac{0.0256}{1.0256} = 2.50\ \text{wt.\%} \quad (3)$$

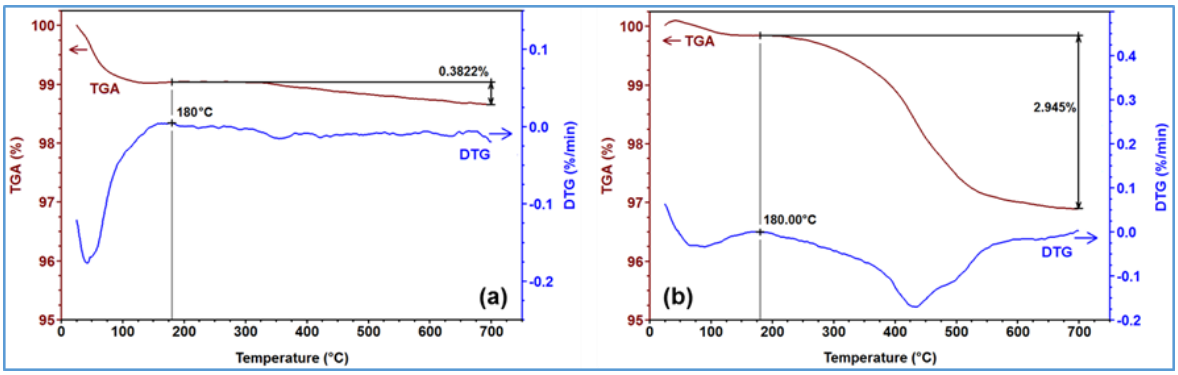

Figure 3.3. (a): TGA and (b) DTG curves of $oZrO_2$ and $mZrO_2$ nanoparticles.

3.1.3. Field Emission Scanning Electron Microscopy and dynamic light scattering

Figure 3.4 and Fig.3.5 are the FESEM+ images of 2 types of ZrO_2 nanoparticles. The FESEM images of $oZrO_2$ and $mZrO_2$ all demonstrate that the zirconia nanoparticles have size in range from 50 to 140 nm with nanocrystal morphology. The size and shape of the $mZrO_2$ particles after modification are similar to the original ZrO_2 nanoparticles ($oZrO_2$).

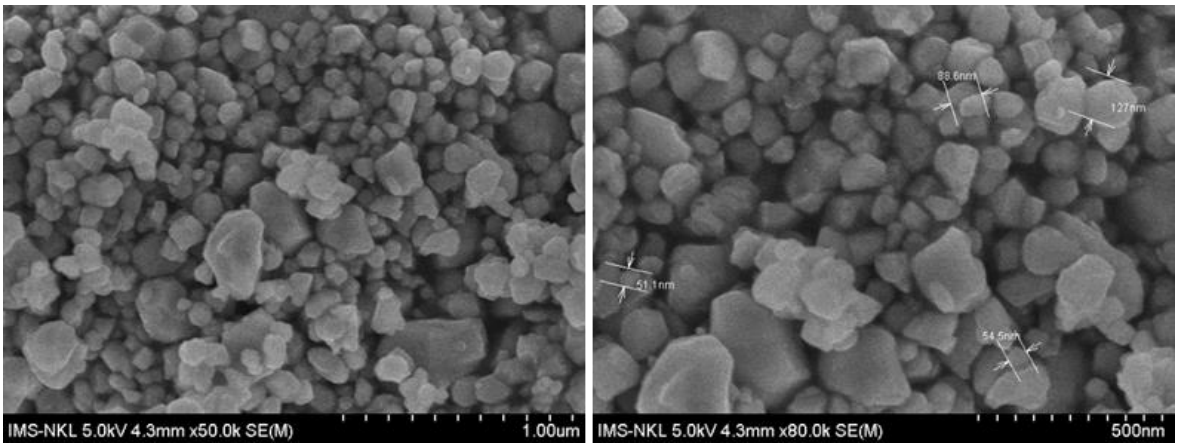

Figure 3.4: FESEM images of $oZrO_2$ nanoparticles.

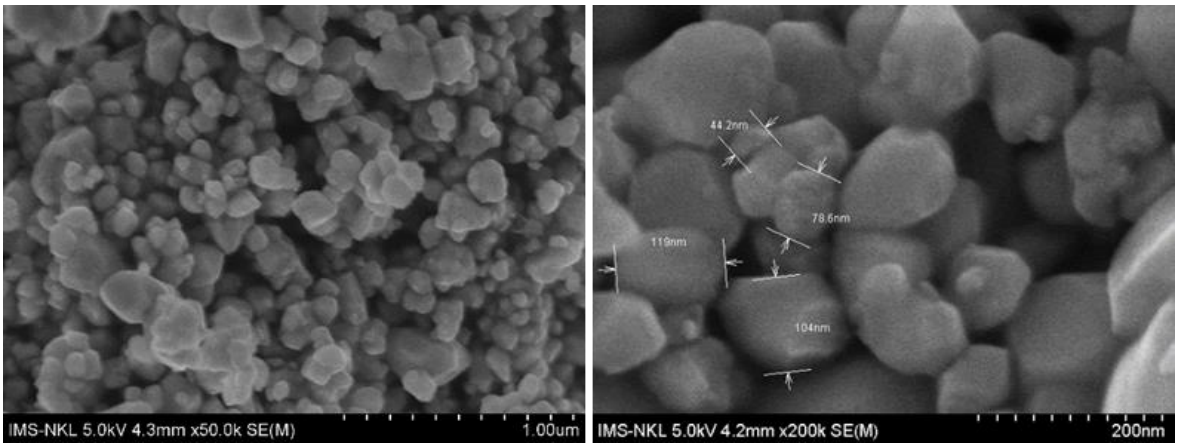

Figure 3.5: FESEM images of $mZrO_2$ nanoparticles.

Figure 3.6 represents the DLS diagrams that display the particle size distribution of the 2 kinds of zirconia nanoparticles in isopropanol. Figure 3.6

shows that the particle size distributions of $oZrO_2$ and $mZrO_2$ nanoparticles are in the range of 80 – 400 with relatively low polydispersity indexes (PdI) of 0.127 and 0.283, respectively. The Z-average size of $oZrO_2$ and $mZrO_2$ are 138.6 nm and 154.5 nm, respectively. These values are higher than those observed by FESEM. This is a common phenomenon because of Z-average is a measurement of hydrodynamic particle size while FESEM is a direct visual of particle size [69–71].

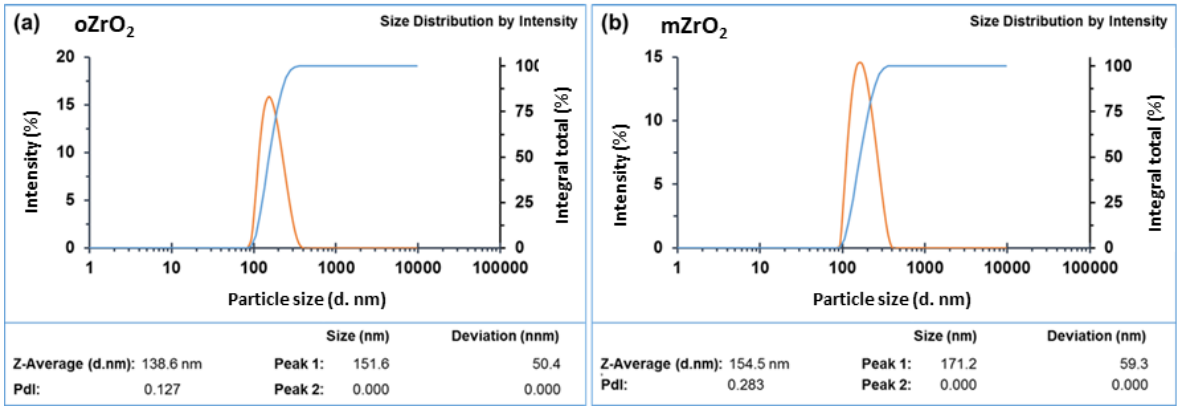

Figure 3.6: DLS diagrams of (a): $oZrO_2$ and (b): $mZrO_2$ nanoparticles.

3.1.4. The crystalline structures of samples

Figure 3.7 displays the XRD patterns of $oZrO_2$ and $mZrO_2$ samples which indicate the same diffraction peaks at 2θ angles. Table 3.1 is the XRD analytical data, showing that the peaks of $oZrO_2$ and $mZrO_2$ are characteristic of the monoclinic crystal structure of zirconia (monoclinic ZrO_2) corresponding to ICCD standard tag 00-037-1484 of baddeleyite (ZrO_2) [72].

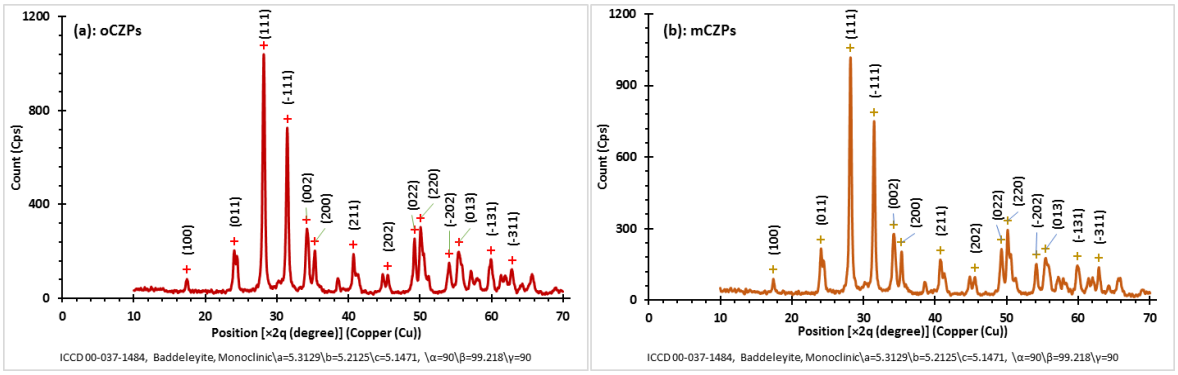

Figure 3.7: XRD patterns of (a): $oZrO_2$ and (b): $mZrO_2$ nanoparticles.

Table 3.1: XRD analysis results of $oZrO_2$ and $mZrO_2$ nanoparticles

STT	$oZrO_2$		$mZrO_2$	
	2θ (°)	**(hkl)**	**2θ (°)**	**(hkl)**
1	17.42	(100)	17.40	(100)
2	24.04	(011)	24.06	(011)
3	28.16	(111)	28.18	(111)
4	31.46	(-111)	31.48	(-111)
5	34.20	(002)	34.24	(002)
6	35.32	(200)	35.30	(200)
7	40.72	(211)	40.72	(211)
8	45.52	(202)	45.56	(202)
9	49.26	(022)	49.26	(022)
10	50.10	(220)	50.12	(220)
11	54.10	(-202)	54.14	(-202)
12	55.44	(013)	55.44	(013)
13	59.94	(-131)	59.86	(-131)
14	62.88	(-311)	62.86	(-311)

3.2. Synthesis and characterization of nanocomposites PMMA-g-ZrO_2 from modified ZrO_2 and MMA monomers

3.2.1. Fourier-transform infrared spectroscopy

Figure 3.8 (c) is the spectrum of the $gZrO_2$ which clearly shows the specific absorption bands of the PMMA grafted onto surfaces of the ZrO_2 particles such as ν(C=O) at 1719 cm^{-1}, ν(–CH_3, OCH_3 and CH_2) vibrations at 2987, 2953 and 2853 cm^{-1}, δ(CH_3) at 1455 cm^{-1}, ν(C-O) at 1167 cm^{-1}, ν(O-C-Si) at 1089 cm^{-1}. The above results indicate that organic moieties such that vinyl groups and PMMA are attached to ZrO_2 particles. This can be explained by the reaction diagrams shown in Figure 3.9 which shows the grafting reaction via the copolymerization of MMA and the vinyl groups on the surface of MPTS-modified ZrO_2 nanoparticles. As a result, PMMA molecules were formed surrounding the ZrO_2 particle. In this case homo PMMA was also formed. However, this homopolymer was almost removed by the extraction process.

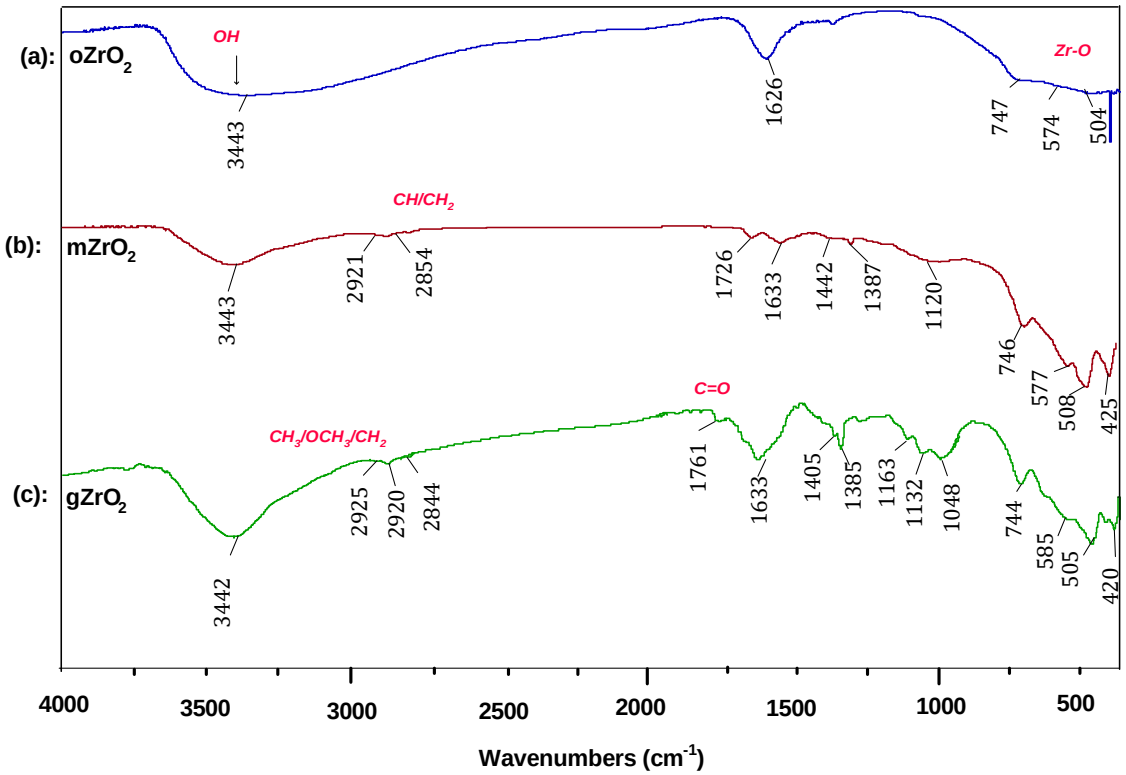

Figure 3.8: FTIR spectra (a) $oZrO_2$, (b) $mZrO_2$ and (c) $gZrO_2$ nanoparticles.

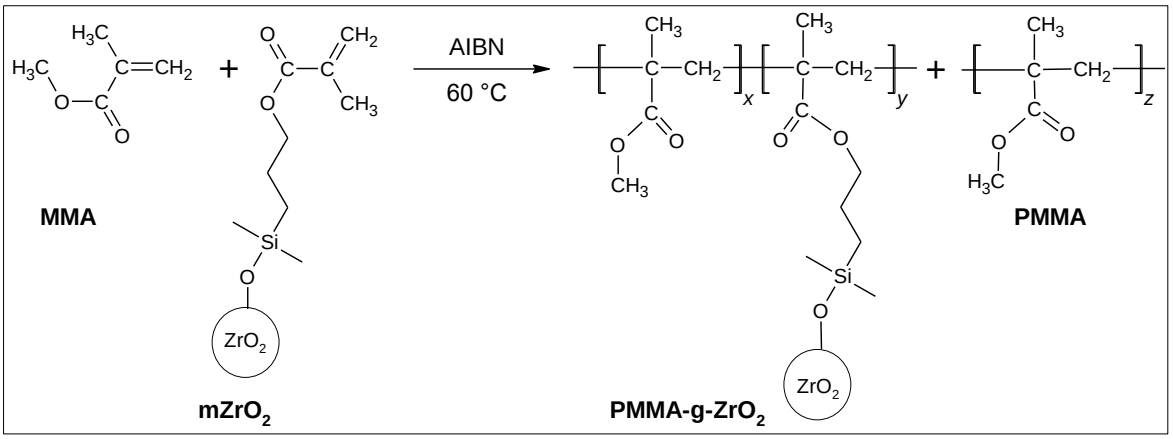

Figure 3.9: Reaction scheme of the formation of PMMA-g-ZrO_2 hybrid nanoparticle.

3.2.2. Thermal Gravimetric Analysis (TGA)

Figure 3.10 displays the TGA and DTG curves of $oZrO_2$, $mZrO_2$ and $gZrO_2$ samples. For the decomposition of $gZrO_2$, its TGA curve also shows the 2 stages. The first stage is the also due to physical water evaporation and the second stage can be attributed to the decomposition of organic MPTS and PMMA in which amount of MPTS can be neglected in compared with that of PMMA. Therefore, PMMA grafted content can be evaluated by the difference of weight changes between 180-700 °C of TGA curve $gZrO_2$ (11.97 %) and

$mZrO_2$ (2.945%) that is 11.97 – 2.945 = 9.03 % (Figure 3.10a) [48]. As mentioned above the physical homo PMMA absorbed onto ZrO_2 can be neglected because it was almost removed through the extraction process.

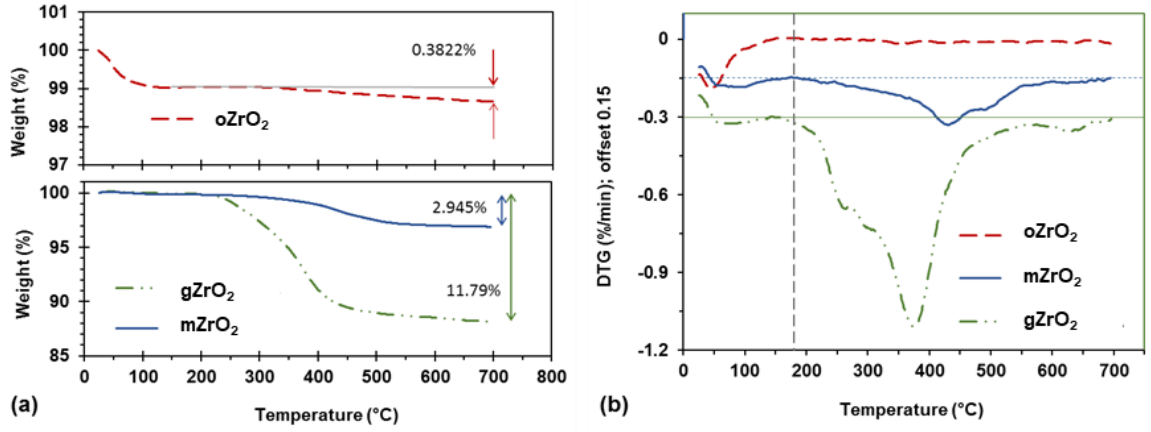

Figure 3.10: TGA and DTG compared with oZrO2 and mZrO2 nanoparticles.

3.2.3. XRD, DLS spectra and FESEM image

Figure 3.11 (a) is XRD spectrum of $gZrO_2$ obtain after extracting PMMA from the synthesized PMMA-g-ZrO_2. Based on XRD analysis, $gZrO_2$ nanoparticles are also in monoclinic or baddeleyite crystalline. The grafting PMMA did not make any change of the crystalline structure of ZrO_2.

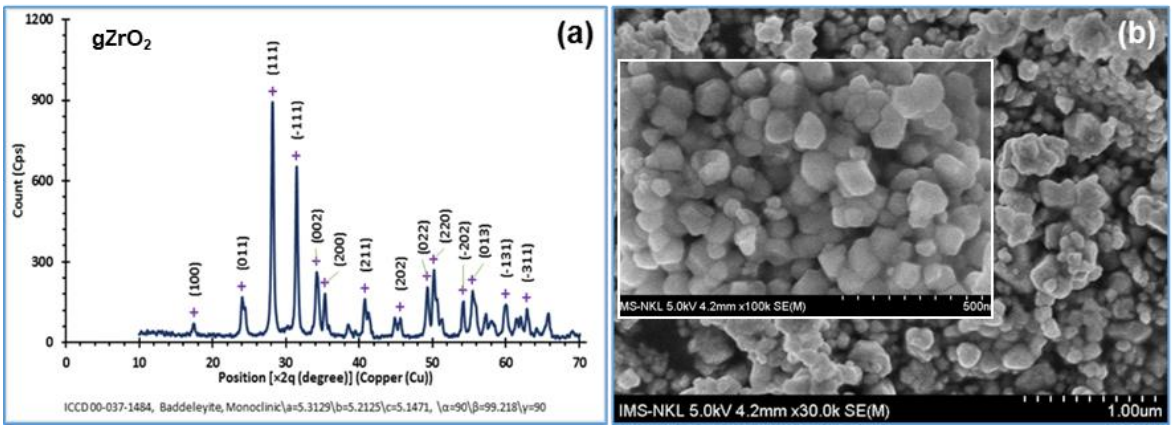

Figure 3.11: (a) XRD spectrum and (b) FESEM image of $gZrO_2$ nanoparticles.

Figure 3.11 (b) is FESEM image of $gZrO_2$ nanoparticles. The FESEM images demonstrate the zirconia nanoparticles have size in range from 50 to 150 nm. It can be suggested that the zirconia particles are cross-linked together through PMMA molecular to form clusters, each cluster comprised of several ZrO_2 primary nanoparticles.

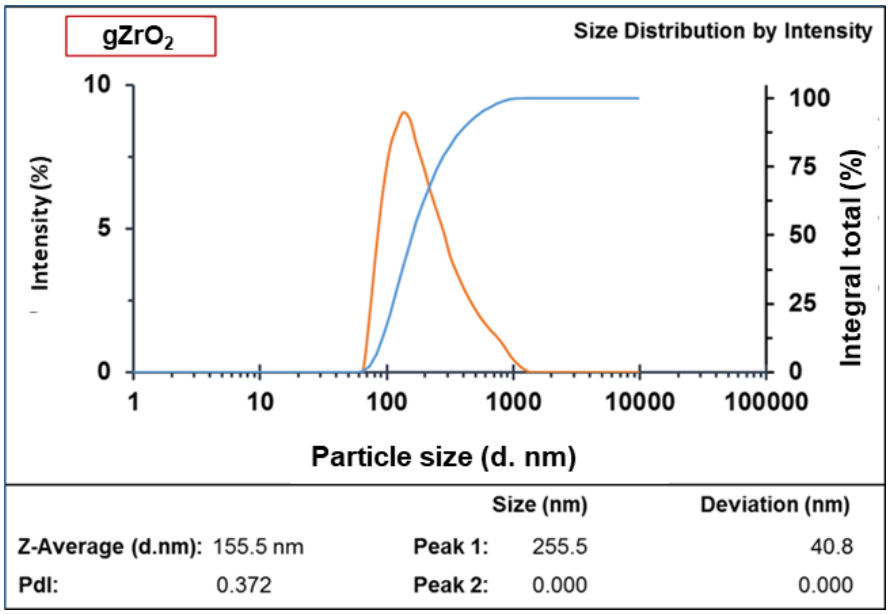

Figure 3.12: DLS curve of $gZrO_2$ nanoparticles.

Figure 3.12 represents the DLS diagrams on the particle size distribution of the grafting zirconia nanoparticles in isopropanol. Figure 3.12 shows that the particle size distribution of $gZrO_2$ is in range (60-1100 nm) with PdI of 0.372; larger than PdI of $oZrO_2$ and $mZrO_2$ in section 3.1.3, meaning that there were some large particles in the $gZrO_2$ sample. It is due to the grafting reaction had conjugated some ZrO_2 nanoparticles together into larger particles. Their average particle size is D_Z = 156 nm, which is also not much larger than that of $oZrO_2$ (138 nm) and $mZrO_2$ (154 nm).

3.3. Fabrication and characterization of 3D printing filaments based on PMMA/ZrO_2 hybrid nanocomposites

3.3.1. Evaluation of extrusion processing conditions

3.3.1.1. Evaluation of processability through visual observation

Table 3.2 represents different temperature profiles and rotor speeds for fabricating PMMA/ZrO_2 3D printing filaments with the same 2.5 wt.% of ZrO_2 loading. For evaluating the influence of temperature profiles, rotor speed was maintained at 80 rpm for all 4 level of temperatures. For evaluating the influence of rotor speeds, T210 temperature profile was applied for all 3 level of speeds, in which the temperatures of 190-200-210-210 °C were set up for 4 zones (as discused later in section 3.3.1.2, the temperature profile of T210 shows the best mechanical properties).

The extruded filaments were drawn with constant speed and scrolled into a spool. The heating zones (from 1 to 4) of the extruder were set at different

temperature profiles, where the lowest temperature is used for the first zone (zone1, the feed zone of the extruder), and the zone3 and die zone and of extruder were set at the same highest temperatures.

Table 3.2: PMMA/ZrO_2 3D printing filaments fabricated at different conditions.

Label for conditions	**Roto speed (rpm)**	**Temperature (°C)**			
		Zone 1	**Zone 2**	**Zone 3**	**Zone 4**
T200	80	180	190	200	200
T210	80	190	200	210	210
T220	80	200	210	220	220
T230	80	210	220	230	230
N60	60	190	200	210	210
N80	80	190	200	210	210
N100	100	190	200	210	210

In which:

+ T200: 3D printing filaments fabricated at 200^{o}C (zone 3 and zone 4);

+ T210: 3D printing filaments fabricated at 210^{o}C (zone 3 and zone 4);

+ T220: 3D printing filaments fabricated at 220^{o}C (zone 3 and zone 4);

+ T230: 3D printing filaments fabricated at 230^{o}C (zone 3 and zone 4);

+ N60, N80, N100: 3D printing filaments fabricated at rotor speed of 60 rpm, 80 rpm and 100 rpm, respectively.

Figure 3.13: PMMA and PMMA/ZrO_2 3D printing filaments.

By visual observation, Table 3.3 shows that using the temperature profile conditions of T210, T220, N80 and N100 can make good products of filaments with relative uniform in diameter, and smooth surface. It should be noted that

the no good filament products were neglected from mechanical testing, only the good filament samples were selected to test the tensile properties.

Table 3.3: Processing ability evaluation 3D printing filaments

Samples	Visual evaluation	Filament appearance
T200	Not Good	Shiny, smooth, non-uniform
T210	*Good*	*Shiny, smooth,* uniform
T220	*Good*	*Shiny, smooth,* uniform
T230	Not Good	Many air bubbles
N60	Not Good	Shiny, smooth, non-uniform
N80	Good	*Shiny, smooth,* uniform
N100	Good	*Shiny, smooth,* uniform

3.3.1.2. Evaluation of processability through mechanical measurements

Table 3.4 represents flexural properties of PMMA/mZrO_2 3D printing filaments (mZrO_2 at 2.5wt.%) prepared at different temperature profiles. The tesing samples were obtained by using molding into the beams as described in Figure 2.3, at least 3 testing beams were prepared for one type of filament extruded with a temperature profile. At the same rotor speed of 80 rpm, the results in Table 3.4 show that the testing beam samples prepared with the temperature profile of T210 exhibits better flexural peoperties, and lower shrinkage in comparison with those of the temperature profile of T220 (the flexural strength and the flexural strain are 7.8% and 41.6% higher, respectively). This can be explained by the temperatures in T220 profile are higher than T210, which caused the thermal degradation of PMMA, some degraded gas were formed in the filament, thus, reducing its flexural properties.

The T210 temperature profile was applied to prepare filament at different rotor speeds (60, 80 and 100 rpm). The flexural properties of the filaments prepared at rotor speeds of 80 rpm are significantly higher than those of filaments that were prepared at 80 and 100 rpm (N60 and N100).

From the visual and mechanical evaluations, it can be concluded that that the processing conditions of T210 and N80 are the most optimal condition for fabricating the 3D printing filaments based on PMMA/ZrO_2 hybrid nanocomposites with good appearance and good mechanical properties.

Table 3.4: Flexural properties of the 3D printing filaments of PMMA/$mZrO_2$ hybrid nanocomposite (at $mZrO_2$ content of 2.5wt.% at different processing conditions

Samples	Flexural modulus (MPa)	Flexural strength (MPa)	Flexural strain (%)	Shrinkage (%)
T210 (N80)	2748	92.9	5.26	1.41
T220 (N80)	2808	86.9	3.15	1.57
N60 (T210)	2748	92.9	5.26	1.41
N80 (T210)	2815	98.6	6.35	1.36
N100 (T210)	2704	91.2	4.93	1.53

3.3.2. Characterization of 3D printing filaments based on PMMA/ZrO_2 hybrid nanocomposite

In this section, the extrusion processing condition of temperature profile of 190-200-210-210 °C and rotor speed of 80 rpm (the combinittion of T210/N80) was applied to fabricate 3D printing filaments based on PMMA/ZrO_2 nanocomposite using $oZrO_2$, $mZrO_2$ and $gZrO_2$ at different contents. Basically, the mechanical properties of the filaments can be determined directly from the 3D printing filaments themselves. However, it is difficult to load the filament samples into the holder of mechanical testing intrument, the obtained results may have very large errors. Therefore, the mechanical properties of the 3D printing filaments were determined through molded samples prepared by using a Haake MiniJet injection molding machine heated at 220 °C with an injection pressure of 600 bar, mold temperature of 100°C [73].

Figure 3.14 represents the flexural properties (flexural strength, flexural strain) of samples from the PMMA/$gZrO_2$ 3D printing filament with $gZrO_2$ contents of 1; 2.5; 5; 7.5 wt.%. Figure 3.14a shows that the flexural strain of the PMMA/ZrO_2 3D printing filaments tends to decrease with ZrO_2 content. However, the flexural strain of PMMA/$gZrO_2$ and PMMA/$mZrO_2$ filaments are about 20-30% and 10-20% higher than that of PMMA/$oZrO_2$ filaments, respectively. A similar trend is also observed, the flexural strength of

PMMA/gZrO$_2$ and PMMA/mZrO$_2$ filaments are about 0.7-3.6% and 0.3-1.8% higher than that of PMMA/oZrO$_2$ filaments. The remarkable results are that the flexural strength of PMMA/gZrO$_2$ and PMMA/mZrO$_2$ filament samples tend to increase compared to neat PMMA filament and reaches maximum value at 1wt.% ZrO$_2$ content (3.6% higher than that of PMMA/oZrO$_2$ 1 wt.% filament), after that their flexural strength tends to decrease as shown in Figure 3.14b.

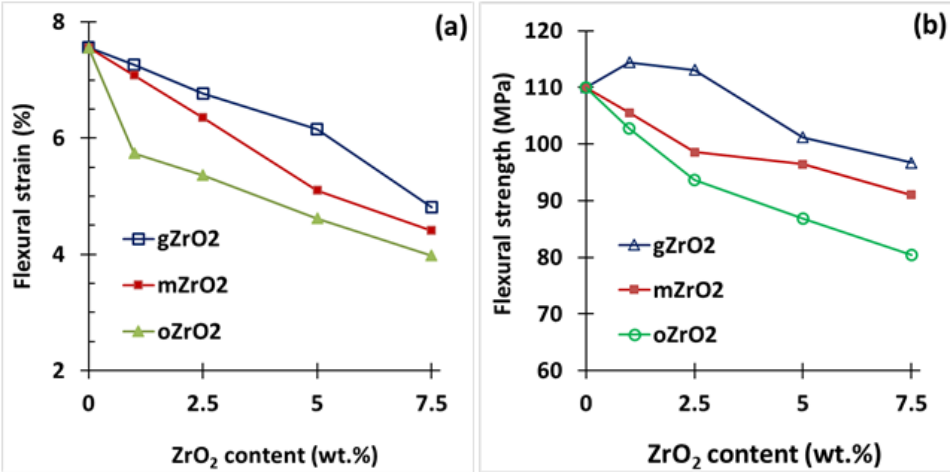

Figure 3.14: Flexural properties of PMMA/ZrO$_2$ 3D printing filaments with different contents of oZrO$_2$, mZrO$_2$, and gZrO$_2$.

Table 3.5, 3.6 and 3.7 represent the flexural properties including the flexural modulus of and the shrinkage (compared to the original length of the mold) of PMMA/oZrO$_2$, PMMA/mZrO$_2$ and PMMA/gZrO$_2$ 3D printing filaments, respectively. Tables 3.5-3.7 show that the flexural modulus of all three kinds of PMMA/ZrO$_2$ 3D printing filaments increases with the ZrO$_2$ content. Meanwhile, the shrinkage of all PMMA/ZrO$_2$ 3D printing filaments tends to decrease with increasing ZrO$_2$ content. This result is also completely reasonable because ZrO$_2$ is a good reinforcing agent for PMMA, especially at the nanoscale. The thermal expansion of ZrO$_2$ is also known as very low, additionally, it can also penetrate into the pores of PMMA matrix and reduce the overall shrinkage of PMMA/ZrO$_2$ hybrid nanocomposite systems.

Table 3.5: Flexural properties of PMMA/oZrO_2 filaments

Samples	Flexural modulus (MPa)	Flexural strength (MPa)	Flexural strain (%)	Shrinkage (%)
PMMA	7.56	110	2755	1.58
PMMA/oZrO_2 (1wt.%)	5.74	102.8	2765	1.41
PMMA/oZrO_2 (2.5wt.%)	5.36	93.7	2789	1.37
PMMA/oZrO_2 (5wt.%)	4.62	86.9	2818	1.33
PMMA/oZrO_2 (7.5wt.%)	3.98	80.4	2869	1.14

Table 3.6: Flexural properties of PMMA/mZrO_2 filaments

Samples	Flexural modulus (MPa)	Flexural strength (MPa)	Flexural strain (%)	Shrinkage (%)
PMMA	7.56	110	2755	1.58
PMMA/mZrO_2 (1wt.%)	7.08	105.5	2774	1.47
PMMA/mZrO_2 (2.5wt.%)	6.35	98.6	2815	1.36
PMMA/mZrO_2 (5wt.%)	5.10	96.4	2868	1.37
PMMA/mZrO_2 (7.5wt.%)	4.41	91.0	2911	1.33

Table 3.7: Flexural properties PMMA/gZrO_2 filaments

Samples	Flexural modulus (MPa)	Flexural strength (MPa)	Flexural strain (%)	Shrinkage (%)
PMMA	7.56	110	2755	1.58
PMMA/gZrO_2 (1wt.%)	7.26	114.4	2785	1.36
PMMA/gZrO_2 (2.5wt.%)	6.76	113.1	2852	1.35
PMMA/gZrO_2 (5wt.%)	6.15	101.2	2919	1.3
PMMA/gZrO_2 (7.5wt.%)	4.81	96.7	2967	1.18

As shown in Figure 3.15a, with increasing content of ZrO_2, the tensile strength of the PMMA/ZrO_2 hybrid nanocomposites decreases. It means the ZrO_2 nanoparticles plays a important role as an inorganic dispersed phase which causes a decrease of the flexibility of PMMA matrix [74]. Therefore, adding ZrO_2 into PMMA matrix leads to decrease physico-mechanical properties of the PMMA 3D printing filaments. Nevertheless, the tensile strength of the PMMA/gZrO_2 filaments was higher (about than that of the PMMA/mZrO_2 filaments and that of the PMMA/oZrO_2 is the lowest, when

compared at the same ZrO_2 content. This indicates that the modification of ZrO_2 nanoparticles is really necessary for the fabrication of the PMMA/ZrO_2 hybrid nanocomposites as well as PMMA/ZrO_2 filaments.

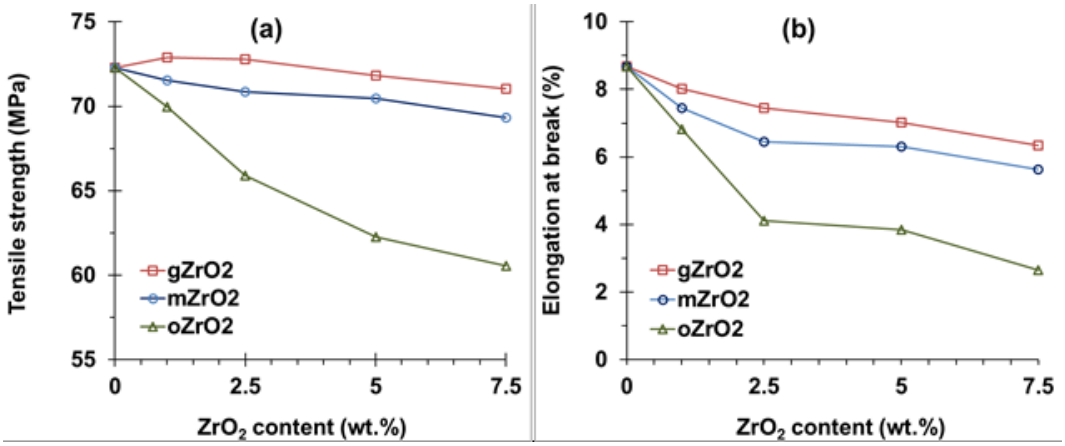

Figure 3.15: Tensile properties of PMMA/ZrO_2 3D printing filaments with different contents of ZrO_2.

Table 3.8: Tensile properties of PMMA ZrO_2 filaments with different contents of ZrO_2 (o, m, gZrO_2)

PMMA/oZrO_2 filaments	oZrO_2				
	0wt.%	1 wt.%	2.5 wt.%	5 wt.%	7.5 wt.%
E-moduls (MPa)	1546 ± 35	1556 ± 26	1563 ± 25	1573 ± 42	1583 ± 14
Elongation at break (%)	8.67 ± 0.5	6.82 ± 1.1	4.11 ± 0.7	3.85 ± 0.8	2.66 ± 0.2
Tensile strength (MPa)	72.3 ± 0.9	70.0 ± 1.6	65.9 ± 1.5	62.3 ± 0.8	60.5 ± 1.1
PMMA/mZrO_2 filaments	mZrO_2				
	0 wt.%	1 wt.%	2.5 wt.%	5 wt.%	7.5 wt.%
E-moduls (MPa)	1546 ± 26	1565 ± 20	1582 ± 30	1600 ± 25	1632 ± 20
Elongation at break (%)	8.67 ± 0.5	7.44 ± 0.2	6.45 ± 0.3	6.31 ± 0.4	5.63 ± 0.5
Tensile strength (MPa)	72.3 ± 0.9	71.55 ± 0.8	70.85 ± 1.2	70.48 ± 1.1	69.32 ± 0.9
PMMA/gZrO_2 filaments	gZrO_2				
	0 wt.%	1 wt.%	2.5 wt.%	5 wt.%	7.5 wt.%
E-moduls (MPa)	1546 ± 26	1566 ± 23	1569 ± 12	1593 ± 22	1636 ± 29
Elongation at break (%)	8.67 ± 0.4	8.67 ± 0.3	8.01 ± 0.3	7.45 ± 0.2	7.02 ± 0.3
Tensile strength (MPa)	72.3 ± 0.9	72.3 ± 0.8	72.9 ± 0.5	72.8 ± 0.6	71.82 0.4

Table 3.8 represents the tensile properties of ZrO_2 materials (o, m, gZrO_2) with different ZrO_2 contents. The results on tensile strength and elongation at break of ZrO_2 have been represented and discussed above in Figure 3.15. Table 3.8 shows that the elastic modulus of 3D printing PMMA/ZrO_2 hybrid filaments ranges from 1556 to 1636 MPa and tends to increase with ZrO_2

content. Among them, PMMA/gZrO_2 filaments show the larger elastic modulus than PMMA/mZrO_2 and PMMA/oZrO_2 filaments.

On observation of the Young's modulus of the PMMA/ZrO_2 in Table 3.8, the obtained results indicates that the Young's modulus of the filament samples ranges from 1555 to 1635 MPa and tend to increase with the ZrO_2 content. Among them, gZrO_2 nanoparticles can strongly increase the Young's modulus of PMMA filament, next is for mZrO_2 nanoparticles.

3.3.3. Field Emission Scanning Electron Microscopy (FESEM image)

Figure 3.16 represents the FESEM images of PMMA/oZrO_2 (5 wt.%) at different magnifications. Most of ZrO_2 nanoparticles disperse well in the PMMA matrix at nanoscale from single particles to a cluster comprised from 2 – 5 nanoparticles with size from 10 to 200 nm. Nevertheless, there are some large clusters, each cluster is comprised of several tens of nanoparticles with size of about 1 - 2 μm. In overall, it can be seen that ZrO_2 nanoparticles are well adhered with the PMMA matrix due to the good interaction polymer layer surrounding the ZrO_2 nanoparticles.

Figures 3.17 and 3.18 show that when treated with MPTS silane or grafting with PMMA, the formation of clusters and amount of particles for each cluster in the PMMA/mZrO_2 and PMMA/gZrO_2 hybrid nanocomposites are reduced. Each cluster comprised of 2 to 5 particles with size less than 200 nm. This can be explained that the modification of ZrO_2 with organic moieties (MPTS and PMMA) has reduced the surface energy of the ZrO_2 nanoparticles, enhancing the organic affinity of the ZrO_2 nanoparticles with the PMMA matrix. As a result, the dispersion of mZrO_2 and gZrO_2 nanoparticles is better than that of oZrO_2 nanoparticles.

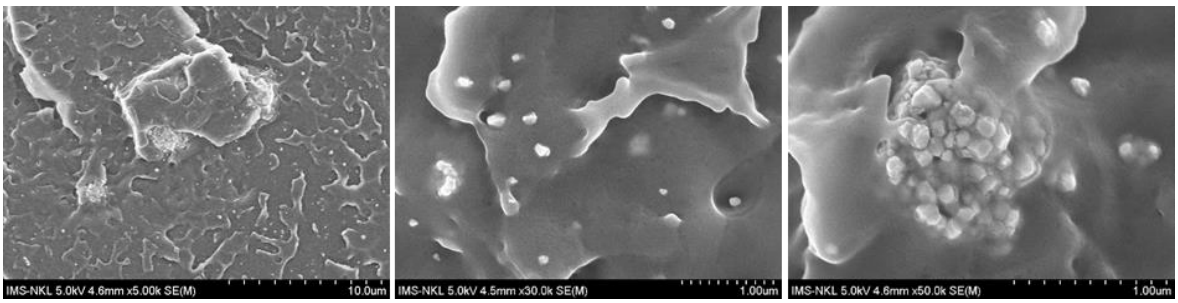

Figure 3.16: FESEM image of PMMA/oZrO_2 filaments 5 wt.%

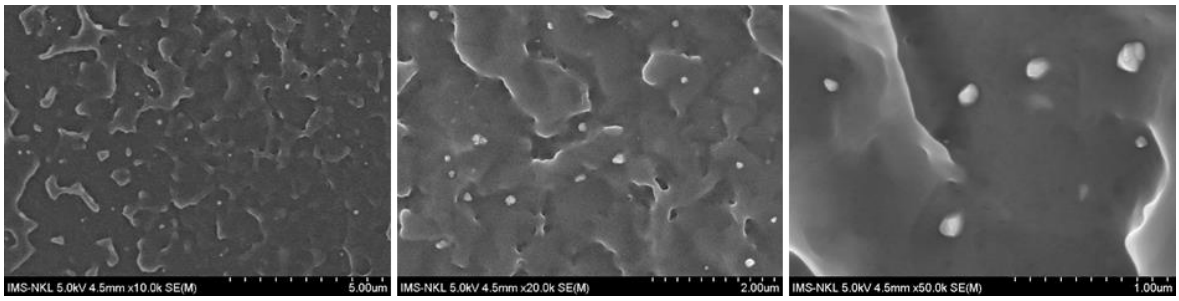

Figure 3.17: FESEM image of PMMA/mZrO_2 filaments 5wt.%

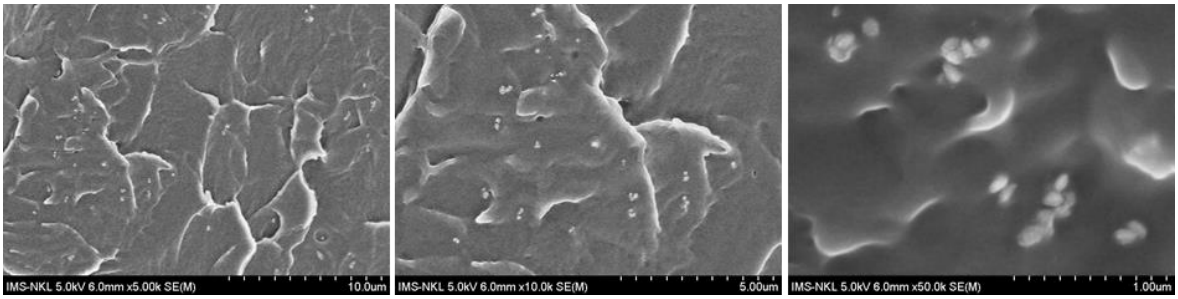

Figure 3.18: FESEM image of PMMA/gZrO_2 filaments 5wt.%

3.4. Characterization of 3D printed samples from PMMA/ZrO_2 filaments

The testing samples from PMMA/gZrO_2 2.5 wt.% is shown in Figure 3.19. The image shows a clear opalescent color due to both the air pore and the radiopacity of ZrO_2.

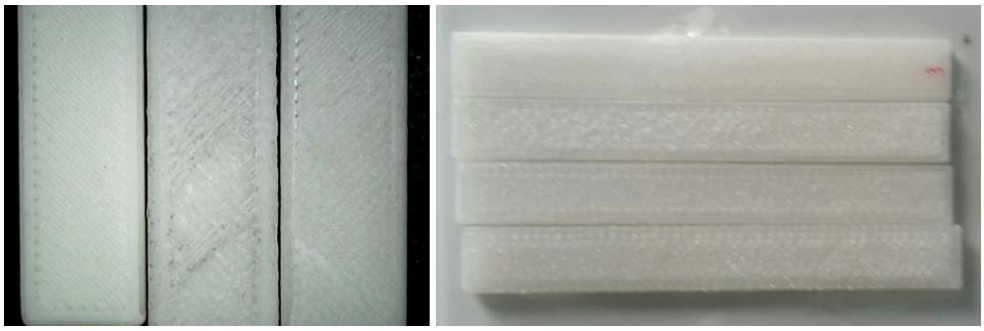

Figure 3.19: Printed specimen in bar (beam) shape prepared by using an FDM 3D printer from PMMA and PMMA/gZrO_2 filaments.

Table 3.9 is the tensile properties of 3D printed beams made by using the FDM 3D printer from PMMA/ZrO_2 hybrid nanocomposite filaments, in this case, the tensile test standard is performed according to ASTM D866 applied to bar/beam shapes. The labels of $\Delta\sigma T$, ΔE and $\Delta\varepsilon T$ are corresponding to the decrements in tensile strength, elastic modulus and elongation at break of printed samples and molded samples prepared from the same kind of filaments. The results show that the tensile strength of the printed samples is quite high, from 38.5 to 43.9 MPa, the elastic modulus is varied from 1119 to 1405 MPa

and the elongation at break is varied from 4.06 to 5. 26 (%). It can also be seen that all tensile strength measurements of the 3D printed samples are smaller than those of the corresponding molded samples. The decrement of Δσ is ranged from 40 to 47 %, the largest is for PMMA and smaller is for samples containing $gZrO_2$. The decrement of ΔBM is ranged from 3.9 to 4.8 %, the largest is for PMMA and smaller is for samples containing $gZrO_2$ (39 – 43 %).

Table 3.9: Tensile properties of 3D printing beams $gZrO_2$

Printed samples	**σ_T (MPa)**	***$\Delta\sigma_T$ (%)***	**E (MPa)**	***ΔE (%)***	**ε_T (%)**	***$\Delta\varepsilon_T$ (%)***
PMMA	38.5	*47* ↓	1119	*28* ↓	5.26	*39* ↓
PMMA/$gZrO_2$ (1wt.%)	42.8	*41* ↓	1275	*19* ↓	4.56	*43* ↓
PMMA/$gZrO_2$ (2.5wt.%)	43.9	*40* ↓	1372	*14* ↓	4.41	*41* ↓
PMMA/$gZrO_2$ (7.5wt.%)	43.1	*40* ↓	1405	*14* ↓	4.06	*42* ↓

Note: E – Elastic moduls, σ_T – tensile strength, ε_T – elongation at break; ΔE, $\Delta\sigma_T$, $\Delta\varepsilon_T$ are correspondingly the reductions of E, σ_T and ε_T.

Table 3.10: Flexural properties of 3D printed beams $gZrO_2$

Printed samples	**Flexural strength (MPa)**	***$\Delta\sigma_B$ (%)***	**Flexural moduls (MPa)**	***ΔBM (%)***	**Flexural strain (%)**	***$\Delta\varepsilon_B$ (%)***
PMMA	103	*10.0* ↓	2652	*4.8* ↓	4.5	*38* ↓
PMMA/$gZrO_2$ (1wt.%)	102	*9.8* ↓	2722	*4.6* ↓	3.81	*44* ↓
PMMA/$gZrO_2$ (2.5wt.%)	95	*6.1* ↓	2793	*4.3* ↓	3.55	*42* ↓
PMMA/$gZrO_2$ (7.5wt.%)	92	*4.9* ↓	2852	*3.9* ↓	2.85	*41* ↓

Table 3.10 is the flexural properties of 3D printed beam samples fabricated by the FDM 3D printing method from the 3D printing filaments based on PMMA/ZrO_2 hybrid nanocomposites. The values Δσ, ΔBM and Δε are the decrements in flexural strength, flexural modulus and flexural strain between printed samples and molded samples. It should be noted that the flexural properties of molded samples have been discussed in aforementioned sections. The results in Table 3.10 show that the flexural strength of the 3D printed beams is still quite high (92 – 103 MPa), the flexural modulus of the 3D printed samples is varied from 2652 to 2852 MPa and the flexural strain is varied from 2.85 to 4.5 (%). It can also be seen that all flexural measurements of the 3D printed samples are smaller than that of the corresponding molded samples

prepared from the same 3D printing filaments. The decrease in Δσ is varied in the range of 4.9 - 10 %, the largest is for PMMA and smaller is for the filaments samples containing $gZrO_2$. The decrease in ΔBM is ranged from 3.9 to 4.8 %, the largest is for PMMA and the smaller is for the samples containing $gZrO_2$, the decrement ΔBM is varied in the range of 38 – 44 %.

In this study, the PMMA/ZrO_2 is view as a biomaterial, which can be used for making a prosthetic implant, or a defected bone. In this case, 3D printing technology show advantages for making a suitable implant for certain patient. Like bone cements, the samples are recommended under testing with ISO 5833:2002 standard, in which the required flexural strength and modulus of PMMA acrylic bone cements are 50 MPa and 1800 MPa, respectively. Table 3.10 reveals that the flexural strength and flexural modulus of the 3D-printed testing samples are much higher than those of the required values in the ISO 5833:2002 standard. This suggests that 3D printing technology can be applied for making acrylic resin implants.

CONCLUSIONS AND RECOMMENDATIONS

CONCLUTIONS

- MPTS-modified nanoparticles ($mZrO_2$) have been synthesized by using silanization method at pH 8.5 and room temperature for 24 h. DLS indicated the nanodistribution of $mZrO_2$ with average size of 155.5 nm with relatively low polydispersity index (0.283). FTIR and TGA indicated that the MPTS was grafted onto the surface of the ZrO_2 with the grafting percentage of 2.5 wt.%.

- PMMA-grafted ZrO_2 nanoparticles ($gZrO_2$) have been synthesized via copolymerization between MMA and $mZrO_2$ at 60°C for 8 h, the grafting percentage of PMMA onto the surface of the ZrO_2 was evalueted as 9.03 wt.% by TGA. The DLS patterns showed that the polydispersity index and particle size distribution of $gZrO_2$ nanoparticles were higher compared with $mZrO_2$ nanoparticles. FESEM images and XRD patterns indicated primary ZrO_2 nanoparticles did not change after silanization and PMMA grafting.

- The 3D printing PMMA/ZrO_2 nanocomposite filaments have been fabricated via melt extrusion process using origin ZrO_2 ($oZrO_2$), $mZrO_2$ and $gZrO_2$ as fillers with contents from 1 to 7.5wt.% at temperature profile of 190-200-210-210 °C and rotor speed of 80 rpm. The flexural strength and modulus as well as tensile strength and modulus of PMMA/$mZrO_2$ and PMMA/$gZrO_2$ filamments were higher than those of PMMA/$oZrO_2$ filamments. FESEM studies showed that $oZrO_2$, $mZrO_2$ and $gZrO_2$ nanoparticles dispersed well in the PMMA matrix in nanoscale despite of some micron size clusters.

- The printed samples from the PMMA/ZrO_2 nanocomposite filaments still exhibited relative high values of tensile and flexural properties. The flexural strength and modulus of printed samples were varied in the ranged of 92-102 MPa and 2722 – 2852 MPa, respectively. The PMMA/ZrO_2 hybrid nanocomposite filaments can be applied to prepare acrylic prosthetic implants with relative high mechanical properties.

RECOMMENDATIONS

- Improvement of the fabrication of the PMMA/ZrO_2 3D printing filaments in large scale for commercial purpose;

- Evaluation of cytotoxicity of the PMMA/ZrO_2 3D printing filaments should be further investigated.

LIST OF PUBLISHED PAPERS BY AUTHOR

1. ***Nguyen Thi Dieu Linh***, Do Quang Tham, Nguyen Vu Giang, Tran Huu Trung, Le Thi My Hanh, Nguyen Thi Thu Trang, Nguyen Thuy Chinh, Tran Thi Mai, Thai Hoang and Do Van Sy. "Synthesis and characterization of monodisperse hydrous colloidal zirconia nanoparticles". Communications in Physics, Vol. 30, No. 4 (2020), pp. 391-398.

2. ***Nguyen Thi Dieu Linh***, Nguyen Thi Kim Dung, Do Quang Tham, Dam Xuan Thang. The Synthesis and characterization of PMMA-grafted-ZrO_2 hybrid nanoparticles. Vietnam Journal of Science and Technology, 2022. (Accepted).

REFERENCES

1. Pandey M., Choudhury H., Fern J. L. C., Kee A. T. K., Kou J., Jing J. L. J., Her H. C., Yong H. S., Ming H. C., Bhattamisra S. K., Gorain B., 2020, 3D printing for oral drug delivery: a new tool to customize drug delivery, *Drug Delivery and Translational Research*, 10(4), 986-1001.
2. Cui M., Pan H., Su Y., Fang D., Qiao S., Ding P., Pan W., 2021, Opportunities and challenges of three-dimensional printing technology in pharmaceutical formulation development, *Acta Pharmaceutica Sinica B*, 11(8), 2488-2504.
3. Chen J., Zhang Z., Chen X., Zhang C., Zhang G., Xu Z., 2014, Design and manufacture of customized dental implants by using reverse engineering and selective laser melting technology, *The Journal of Prosthetic Dentistry*, 112(5), 1088-1095.
4. Oliveira T. T., Reis A. C., 2019, Fabrication of dental implants by the additive manufacturing method: A systematic review, *The Journal of Prosthetic Dentistry*, 122(3), 270-274.
5. Gao C., Wang C., Jin H., Wang Z., Li Z., Shi C., Leng Y., Yang F., Liu H., Wang J., 2018, Additive manufacturing technique-designed metallic porous implants for clinical application in orthopedics, *RSC Advances*, 8(44), 25210-25227.
6. Chen R. K., Jin Y.-a., Wensman J., Shih A., 2016, Additive manufacturing of custom orthoses and prostheses—A review, *Additive Manufacturing*, 12, 77-89.
7. Esmi A., Jahani Y., Yousefi A. A., Zandi M., 2019, PMMA-CNT-HAp nanocomposites optimized for 3D-printing applications, *Materials Research Express*, 6(8), 085405.
8. Stansbury J. W., Idacavage M. J., 2016, 3D printing with polymers: Challenges among expanding options and opportunities, *Dental Materials*, 32(1), 54-64.
9. Mendes-Felipe C., Oliveira J., Etxebarria I., Vilas-Vilela J. L., Lanceros-Mendez S., 2019, State-of-the-Art and Future Challenges of UV Curable Polymer-Based Smart Materials for Printing Technologies, *Advanced Materials Technologies*, 4(3), 1800618.
10. Wagner A., Kreuzer A. M., Göpperl L., Schranzhofer L., Paulik C., 2019, Foamable acrylic based ink for the production of light weight parts by inkjet-based 3D printing, *European Polymer Journal*, 115, 325-334.
11. Gad M. M., Abualsaud R., Rahoma A., Al-Thobity A. M., Al-Abidi K. S., Akhtar S., 2018, Effect of zirconium oxide nanoparticles addition on the optical and tensile properties of polymethyl methacrylate denture base material, *International Journal of Nanomedicine*, 13, 283-292.
12. Hu Y., Gu G., Zhou S., Wu L., 2011, Preparation and properties of transparent PMMA/ZrO_2 nanocomposites using 2-hydroxyethyl methacrylate as a coupling agent, *Polymer*, 52(1), 122-129.

13. Reyes-Acosta M. A., Torres-Huerta A. M., Domínguez-Crespo M. A., Flores-Vela A. I., Dorantes-Rosales H. J., Ramírez-Meneses E., 2015, Influence of ZrO_2 nanoparticles and thermal treatment on the properties of PMMA/ZrO_2 hybrid coatings, *Journal of Alloys and Compounds*, 643, S150-S158.
14. Rayna T., Striukova L., 2016, From rapid prototyping to home fabrication: How 3D printing is changing business model innovation, *Technological Forecasting and Social Change*, 102, 214-224.
15. Jasveer S., Jianbin X., 2018, Comparison of Different Types of 3D Printing Technologies, *International Journal of Scientific and Research Publications*, 8(4), 1-9.
16. Berman B., 2012, 3-D printing: The new industrial revolution, *Business horizons*, 55(2), 155-162.
17. Attaran M., 2017, The rise of 3-D printing: The advantages of additive manufacturing over traditional manufacturing, *Business horizons*, 60(5), 677-688.
18. Mạnh Quân N., 2017, In 3D-Công nghệ đỉnh cao của sự phát triển, *Tạp chí Khoa học và Công nghệ Việt Nam*, 10, 37-40.
19. Moreau C., Zeijderveld J. V., 2018, State of 3D Printing 2018: The rise of metal 3D printing, DMLS, and finishes, *Sculpteo's 4th annual report on 3D Printing and Digital Manufacturing*.
20. Statista, 2018, *Worldwide most used 3D printing materials, as of July 2018*, https://www.statista.com/statistics/800454/worldwide-most-used-3d-printing-materials/, Statista GmbH, Johannes-Brahms-Platz 1, 20355 Hamburg, Germany.
21. Parandoush P., Lin D., 2017, A review on additive manufacturing of polymer-fiber composites, *Composite Structures*, 182, 36-53.
22. Ngo T. D., Kashani A., Imbalzano G., Nguyen K. T. Q., Hui D., 2018, Additive manufacturing (3D printing): A review of materials, methods, applications and challenges, *Composites Part B: Engineering*, 143, 172-196.
23. Wittbrodt B., Pearce J. M., 2015, The effects of PLA color on material properties of 3-D printed components, *Additive Manufacturing*, 8, 110-116.
24. Wang X., Jiang M., Zhou Z., Gou J., Hui D., 2017, 3D printing of polymer matrix composites: A review and prospective, *Composites Part B: Engineering*, 110, 442-458.
25. Nematollahi M., Jahadakbar A., Mahtabi M. J., Elahinia M., 2019, in M. Niinomi, *Metals for Biomedical Devices (Second Edition)*, Woodhead Publishing, 331-353.
26. Duda T., Raghavan L. V., 2016, 3D Metal Printing Technology, *IFAC-PapersOnLine*, 49(29), 103-110.
27. Ronca A., Maiullari F., Milan M., Pace V., Gloria A., Rizzi R., De Santis R., Ambrosio L., 2017, Surface functionalization of acrylic based

photocrosslinkable resin for 3D printing applications, *Bioactive Materials*, 2(3), 131-137.
28. Dung H. T., 2018, Fabrication and characterization of supercapacitor electrode by 3D printing, *Vietnam Journal of Science and Technology*, 56(5), 574-581.
29. Palanisamy P., Chavali M., Kumar E. M., Etika K. C., 2020, *Chapter 10 - Hybrid nanocomposites and their potential applications in the field of nanosensors/gas and biosensors*, in K. Pal and F. Gomes, *Nanofabrication for Smart Nanosensor Applications*, Elsevier, 253-280.
30. Roy S., Singha N. R., 2017, Polymeric Nanocomposite Membranes for Next Generation Pervaporation Process: Strategies, Challenges and Future Prospects, *Membranes*, 7(3), 53.
31. de Oliveira A. D., Beatrice C. A. G., 2018, in S. Subbarayan, *Nanocomposites-Recent Evolutions*, InTechOpen, London, 103-127.
32. Naz A., Kausar A., Siddiq M., Choudhary M. A., 2016, Comparative Review on Structure, Properties, Fabrication Techniques, and Relevance of Polymer Nanocomposites Reinforced with Carbon Nanotube and Graphite Fillers, *Polymer-Plastics Technology and Engineering*, 55(2), 171-198.
33. Tavares M. I. B., da Silva E. O., da Silva P. R., de Menezes L. R., 2017, in M.S. Seehra, *Nanostructured Materials: Fabrication to Applications*, IntechOpen, London, 135-151.
34. Canetti M., Scafati S. T., Cacciamani A., Bertini F., 2012, Influence of hydrogenated oligo(cyclopentadiene) on the structure and the thermal degradation of polypropylene-based nanocomposites, *Polymer Degradation and Stability*, 97(1), 81-87.
35. Rousseaux D. D. J., Sallem-Idrissi N., Baudouin A.-C., Devaux J., Godard P., Marchand-Brynaert J., Sclavons M., 2011, Water-assisted extrusion of polypropylene/clay nanocomposites: A comprehensive study, *Polymer*, 52(2), 443-451.
36. Wang B., Wilkes G. L., 1991. New Ti-PTMO and Zr-PTMO ceramer hybrid materials prepared by the sol gel method: Synthesis and characterization, *Journal of Polymer Science Part A: Polymer Chemistry*, 29(6), 905-909.
37. Tavares M. R., de Menezes L. R., do Nascimento D. F., Souza D. H. S., Reynaud F., Marques M. F. V., Tavares M. I. B., 2016, Polymeric nanoparticles assembled with microfluidics for drug delivery across the blood-brain barrier, *The European Physical Journal Special Topics*, 225(4), 779-795.
38. Valentim A. C. S., Tavares M. I., da Silva E. O., 2013, The effect of the Nb2O5 dispersion on ethylene vinyl acetate to obtain ethylene vinyl acetate/Nb2O5 nanostructured materials, *Journal of Nanoscience and Nanotechnology*, 13(6), 4427-32.

39. Xi G. X., Song S. L., Liu Q., 2005, Catalytic effects of sulfates on thermal degradation of waste poly(methyl methacrylate), *Thermochimica Acta*, 435(1), 64-67.
40. Harper C. A., Petrie E. M., 2004, Plastics materials and processes - a concise encyclopedia - Book Review, *IEEE Electrical Insulation Magazine*, 20(4), 47-48.
41. Van Krevelen D. W., Te Nijenhuis K., 2009, *Properties of polymers: their correlation with chemical structure; their numerical estimation and prediction from additive group contributions*, UK, Elsevier, London.
42. Grelle P. F. (2006), *Handbook of Plastic Processes*, John Wiley & Sons, Canada, 1-123.
43. Park J. H., Hwang D. K., Lee J., Im S., Kim E., 2007, Studies on poly(methyl methacrylate) dielectric layer for field effect transistor: Influence of polymer tacticity, *Thin Solid Films*, 515(7), 4041-4044.
44. Soleymani Eil Bakhtiari S., Bakhsheshi-Rad H. R., Karbasi S., Tavakoli M., Hassanzadeh Tabrizi S. A., Ismail A. F., Seifalian A., RamaKrishna S., Berto F., 2021, Poly(methyl methacrylate) bone cement, its rise, growth, downfall and future, *Polymer International*, 70(9), 1182-1201.
45. Geng K., Tsui O., 2016, Effects of Polymer Tacticity and Molecular Weight on the Glass Transition Temperature of Poly(methyl methacrylate) Films on Silica, *Macromolecules*, 49.
46. Bhat G., Kandagor V., 2014, in D. Zhang, *Advances in Filament Yarn Spinning of Textiles and Polymers*, Woodhead Publishing, 3-30.
47. Vernieuwe K., Lommens P., Martins J. C., Van Den Broeck F., Van Driessche I., De Buysser K., 2013, Aqueous ZrO_2 and YSZ Colloidal Systems through Microwave Assisted Hydrothermal Synthesis, *Materials (Basel, Switzerland)*, 6(9), 4082-4095.
48. Bao L., Li X., Wang Z., Li J., 2018, Fabrication and characterazation of functionalized zirconia microparticles and zirconia-containing bone cement, *Materials Research Express*, 5(7), 075404.
49. Duan G., Zhang C., Li A., Yang X., Lu L., Wang X., 2008, Preparation and characterization of mesoporous zirconia made by using a poly (methyl methacrylate) template, *Nanoscale research letters*, 3(3), 118.
50. Liu Z., Tang Y., Kang T., Rao M., Li K., Wang Q., Quan C., Zhang C., Jiang Q., Shen H., 2015, Synergistic effect of HA and BMP-2 mimicking peptide on the bioactivity of HA/PMMA bone cement, *Colloids and Surfaces B: Biointerfaces*, 131, 39-46.
51. Arturo S., *Comprehensive Guide on Polymethyl methacrylate (PMMA or Acrylic)*, 2022; Accessed on 25 Aug 2022, https://omnexus.specialchem.com/selection-guide/polymethyl-methacrylate-pmma-acrylic-plastic.
52. Sabu T., Preetha B., Sreekala M. S., 2018, in K. Shanmugam and R. Sahadevan, *Fundamental biomaterials: ceramics*, Elsevier, UK, 1-46.

53. 911Metallurgist, *Making Zirconia by Zirconium Chlorination*, 2021; 25 Aug 2022, https://www.911metallurgist.com/making-zirconia/.
54. Fedorov P. P., Yarotskaya E. G., 2021, Zirconium dioxide. Review, *Condensed Matter and Interphases*, 23(2), 169-187.
55. El-Barawy K. A., Morsi I. M., El-Tawil S. Z., Francis A. A., *Chlorination of zirconium bearing materials to produce high purity zirconia*, in *AIME 126 Th., SME Annual Meeting and Exhibit*. 1997: Denver, Colorado-USA.
56. Nature News, 1917, The Use of Zirconia as a Refractory Material, *Nature*, 99(2488), 375-376.
57. Domingo-Roca R., Jackson J. C., Windmill J. F. C., 2018, 3D-printing polymer-based permanent magnets, *Materials & Design*, 153, 120-128.
58. Malik H. H., Darwood A. R. J., Shaunak S., Kulatilake P., El-Hilly A. A., Mulki O., Baskaradas A., 2015, Three-dimensional printing in surgery: a review of current surgical applications, *Journal of Surgical Research*.
59. Polzin C., Spath S., Seitz H., 2013, Characterization and evaluation of a PMMA-based 3D printing process, *Rapid Prototyping Journal*, 19(1), 37-43.
60. Dung H. T., Dung T. Q., Huy N. T., Yến N. T., 2017, Building a 3D printer for rapid prototyping using plastic materials, *Tạp chí Khoa học và Công nghệ Đại học Công nghiệp Hà Nội*, 39(4), 72-77.
61. Tung D. T., Dung H. T., 2019, Study on fast charger for 5V 1500F supercapacitor module from photovoltaic panel, *Vietnam Journal of Science and Technology*, 57(1), 82-91.
62. Tam L. T. T., Hung N. V., Tung D. T., Dung N. T., Dung H. T., Dung N. T., Minh P. N., Hong P. N., Lu L. T., 2019, Synthesis and electrochemical properties of porous CNTs-ferrite hybrid nanostructures for supercapacitor, *Vietnam Journal of Science and Technology*, 57(1), 58-66.
63. Lan P. X., Lee J. W., Seol Y.-J., Cho D.-W., 2009, Development of 3D PPF/DEF scaffolds using micro-stereolithography and surface modification, *Journal of Materials Science: Materials in Medicine*, 20(1), 271-279.
64. Park H.-S., Dang X.-P., 2017, Development of a Smart Plastic Injection Mold with Conformal Cooling Channels, *Procedia Manufacturing*, 10, 48-59.
65. Tran N.-H., Nguyen V.-N., Ngo A.-V., Nguyen V.-C., 2017, Study on the Effect of Fused Deposition Modeling (FDM) Process Parameters on the Printed Part Quality, *Int. Journal of Engineering Research and Application*, 7(12), 71-77.
66. Intellectual property office of Vietnam, *wopublish-search "in 3D"*, 2022; 27 Aug 2022, http://wipopublish.ipvietnam.gov.vn/wopublish-search/public/patents?9&query=*:*.
67. Yang J., Liao M., Hong G., Dai S., Shen J., Xie H., Chen C., 2020, Effect of APTES- or MPTS-Conditioned Nanozirconia Fillers on Mechanical

Properties of Bis-GMA-Based Resin Composites, *ACS Omega*, 5(50), 32540-32550.
68. Dick A., Bhandari B., Prakash S., 2019, 3D printing of meat, *Meat Science*, 153, 35-44.
69. Li D., Yao J., Liu B., Sun H., van Agtmaal S., Feng C., 2019, Preparation and characterization of surface grafting polymer of ZrO2 membrane and ZrO2 powder, *Applied Surface Science*, 471, 394-402.
70. Tham D. Q., Huynh M. D., Linh N. T. D., Van D. T. C., Cong D. V., Dung N. T. K., Trang N. T. T., Lam P. V., Hoang T., Lam T. D., 2021, PMMA Bone Cements Modified with Silane-Treated and PMMA-Grafted Hydroxyapatite Nanocrystals: Preparation and Characterization, *Polymers*, 13(22), 3860.
71. Johnson C. S., Gabriel D. A., 2018, in B.J. E., *Spectroscopy in Biochemistry*, CRC Press, 177-248.
72. Song Y. L., 2020, Trends in prosthodontics of dental implantology, *Chinese journal of stomatology*, 55(11), 809-813.
73. Yao T., Deng Z., Zhang K., Li S., 2019, A method to predict the ultimate tensile strength of 3D printing polylactic acid (PLA) materials with different printing orientations, *Composites Part B: Engineering*, 163, 393-402.
74. McMurdie H. F., Morris M. C., Evans E. H., Paretzkin B., Wong-Ng W., Ettlinger L., Hubbard C. R., 2013, Standard X-Ray Diffraction Powder Patterns from the JCPDS Research Associateship, *Powder Diffraction*, 1(2), 64-77.